EXPERIMENTAL MODAL ANALYSIS OF STAR-SPAR BUOY USING EIGENSYSTEM REALIZATION ALGORITHM AND STOCHASTIC SUBSPACE IDENTIFICATION METHODS

BY

PENGYU ZHANG

A THESIS SUBMITTED IN PARTIAL FULFILLMENT OF THE

REQUIREMENTS FOR THE DEGREE OF

MASTER OF SCIENCE

IN

OCEAN ENGINEERING

UNIVERSITY OF RHODE ISLAND

2012

MASTER OF SCIENCE THESIS

OF

PENGYU ZHANG

APPROVED:

Thesis Committee:

Major Professor Sau-Lon James Hu

Harold T. vincent

George Tsiatas

Nasser H. Zawia

DEAN OF THE GRADUATE SCHOOL

UNIVERSITY OF RHODE ISLAND

2012

ABSTRACT

The star-spar buoy employed in this study is a small buoy system for omni-directional wave energy harvesting, and it has been designed for the system to resonate at a dominant period of 2.25 seconds in heave motion. However, this design frequency must be verified through experiments. The objective of this study is thus to obtain the frequency and damping, associated with the heave motion of the star-spar buoy through tank and sea experiments. Two specific time domain modal identification techniques to be utilized in this study are eigensystem realization algorithm (ERA) and stochastic subspace identification (SSI). ERA is a deterministic (input-output) modal identification technique and SSI is a stochastic (output-only) technique.

Traditionally, the discrete Fourier transform of a digital signal has been employed as a signal decomposition technique, as well as a modal identification technique by picking the peaks from its Fourier spectrum. However, the purposes and concepts of signal decomposition and modal identification are very different. While the performance of a signal decomposition technique would be judged based on the fitting between the reconstructed signal and the original signal, that of a modal identification technique could be judged based on whether identified modal parameters are close to the true modal parameters. When true modal parameters are unknown, the performance of a modal identification technique usually would be judged based on a stabilization diagram.

When a response signal, from either the tank test or the sea test, is modeled as the sum of many damped harmonic components, the numerical studies in this thesis demonstrates that using ERA to estimate component frequencies and damping ratios, together with a least-squares solution for getting amplitudes and phase angles, is an excellent signal decomposition technique. For modal identification, SSI is found to be better than ERA, and is a very efficient method for both the tank and the sea test data.

In their theoretical derivations, both ERA and SSI methods assume that the dynam-

ic system is a time-invariant linear system. However, the real buoy-fluid system under investigation must be a nonlinear system, thus to apply ERA or SSI, a first approximation is to treat the dynamic system to be piecewise linear, i.e. linear within a short period. In this study, introducing a sliding window is for assuming that the system is linear within the window duration. With this sliding window, an ERA-based time-frequency analysis, in parallel to the short time Fourier transform (STFT), has been conducted. It was concluded that using ERA-based analysis could overcome the frequency resolution and leakage problems.

ACKNOWLEDGMENTS

First of all, I would like to express my sincere gratitude to my advisor Prof. Sau-Lon James Hu for all the guidance and support he provided me during the past year. He gave me this research opportunity and led me to this exciting field. I would also thank Prof. Harold Vincent, for many fruitful discussions and serving on my committee. I wish to express my appreciation for Wenlong Yang and Junfeng Xin from Ocean University of China, for their help with providing useful insight about this project and working with the Matlab computer language. Finally, I would like to acknowledge my parents for their unrelenting support throughout this project and my education in the US.

TABLE OF CONTENTS

Page

LIST OF TABLES

LIST OF FIGURES

Figure		Page

CHAPTER 1

Introduction

1.1 Star-spar buoy

The star-spar buoy employed in this study, designed by the University of Rhode Island (URI) and Electro Standards Laboratories Inc. (ESL), is a small buoy system for omni-directional wave energy harvesting. The targeted application for this system is not large energy production for single units, but instead the development of simple, easily deployable, and storm resilient systems, to provide a renewable wave power source of 1 kW for distributed marine surveillance and instrumentation systems [1]. Shown in Fig.1 is a 1:4 scale model that is to be studied for its dynamic characteristics in this thesis. This star-spar is a self-contained (water tight) resonating buoy, in which a longer central spar is surrounded by shallower, satellite spars, providing both form stability and a reduced overall average draft (necessary to achieve a proper heave resonance period). The longer central spar, equipped with an embedded Linear Electric Generator (LEG) whose armature motion is excited primarily by the buoys wave-induced heave. Hence, LEG oscillations are maximized by matching buoy heave and LEG natural periods.

Figure 1. Star-spar buoy model

The employed star-spar buoy has been designed for the system to resonate at a dominant period of 2.25 seconds. However, this design frequency must be verified through experiments. Beside the system frequency, another important design parameter which would effect the efficiency of the power generator is the damping of the buoy system as the damping would reduce the amplitude of the oscillation of the buoy system [2]. The only way to find out the damping of the system is through experiments. In other words, it requires dealing with an inverse problem mathematically, that is, to estimate the system parameters from the measured response time history of the buoy.

1.2 Experimental modal analysis

The main objective of this study is to obtain the frequency and damping associated with the heave motion of the star-spar buoy through tank and field experiments. Experimental modal analysis (EMA) [3, 4] is a process of determining the modal parameters (natural frequencies, damping factors and mode shapes) of a dynamic system using the measured data. With the estimated modal parameters, we can validate and update analytical and numerical models, and also gain the knowledge of the true dynamics of the designed structure, thus also monitor the health of the structure [5]. In the past decades, many modal parameter identification methods have been developed, and they can be divided into two broad categories: frequency domain and time domain methods. Early methods of modal identification were developed for the frequency domain. The simplest frequency approach to estimate the modal parameters of a structure subjected to ambient loading is the so-called peak-picking (PP) method [6]. The basic peak-picking method finds the eigenfrequencies as the peaks of non-parametric spectrum estimates. This frequency selection procedure becomes a subjective task in case of noisy operational data, weakly excited modes and relatively close eigenfrequencies. Furthermore, for damping estimation, the related half-power bandwidth method is not reliable at all. Partially because of limitations in the frequency resolution of spectral estimates and leakage errors in the estimates for the frequency domain methods, the new trend is to employ either input-output or output-only time-domain modal identification methods [7]. Although many time-domain techniques have been employed for estimating the modal properties of mechanical and civil structures, such as cars, aircrafts, bridges, offshore platforms, etc, none of these methods, to the best knowledge of the author, have been utilized for ocean buoys.

To be utilized in this study are two specific time domain modal identification techniques: eigensystem realization algorithm (ERA) and stochastic subspace identification (SSI). ERA is a deterministic (input-output) modal identification technique, while SSI is a stochastic (output-only) technique.

1.3 ERA and SSI methods

Although ERA and SSI techniques are intended for different testing conditions, they share a number of similarities in mathematics. For example, both methods use a state-space model for the equation of motion, both must pre-determine the number of modes that have contributed to measured response signal, and both employ truncated singular value decomposition (TSVD) to reduce the model order. A brief description of both methods is given below to show their similarities and differences, and the detailed description of ERA and SSI methods is provided in chapter 2.

ERA

The eigensystem realization algorithm is a modal analysis technique which generates a system realization using pulse response data. ERA was first proposed by Juang and Pappa (1985) for modal parameter identification and model reduction of linear dynamical systems. In the early eighties when multi-input multi-output (MIMO) testing became popular, ERA was developed to handle MIMO test data. Today, ERA method has become one of the most popular methods in civil engineering applications for experimental modal analysis. Based on a deterministic input-output mathematical model, ERA begins with the discrete-time version of the state-space representation:

$$\begin{aligned} \mathbf{x}_{k+1} &= \mathbf{A}\mathbf{x}_k + \mathbf{B}\mathbf{u}_k \\ \mathbf{y}_k &= \mathbf{C}\mathbf{x}_k \end{aligned} \tag{1}$$

where k is the time index, and $\mathbf{x} \in \mathbb{R}^n$, $\mathbf{u} \in \mathbb{R}^m$ and $\mathbf{y} \in \mathbb{R}^l$ are the state, input, and output vectors, respectively. The system model order is n, number of input m, and number of output l. The eigen values of the system matrix $\mathbf{A} \in \mathbb{R}^{n\times n}$ contain the information of modal frequencies and damping factors. The fact that ERA is based on the Markov parameters (i.e., pulse response) makes it possible to construct a block Hankel matrix as the basis for realization of a discrete-time state-space model. Developed based on the minimum realization theory, ERA identifies $\mathbf{A} \in \mathbb{R}^{n\times n}$ within the similarity transformation. In handling noisy signals, ERA partitions the realized model into principal and perturbational (noise) portions so that the noise portion can be disregarded. Although ERA method was theoretically developed on the basis of the excitation being impulsive loading, ERA method is also theoretically applicable to step relaxation testing. Both impulsive loading and step relaxation testing procedures do not impose external loading to the testing structure after the initial time.

SSI

Output-only modal identification methods became very useful when the input is unknown or unmeasurable. Without the knowledge of the real input, mathematically it is logical to assume that the excitation input is a zero-mean Gaussian white noise process. Because of this random white noise assumption, all output-only modal identification methods fall into the category of stochastic system identification. The stochastic subspace identification (SSI) employed in this study is one of the most advanced stochastic system identification techniques. The major break-through of SSI algorithms happened in 1996 with the publishing of the book by van Overschee and De Moor. SSI is a projection-driven method which has been a proven method for a variety of engineering applications.

When no deterministic forces except the stochastic components (noise) are included, the equation of motion for the dynamic system can be written in a discrete-time stochastic state-space model as:

$$\begin{aligned} \mathbf{x}_{k+1} &= \mathbf{A}\mathbf{x}_k + \mathbf{w}_k \\ \mathbf{y}_k &= \mathbf{C}\mathbf{x}_k + \mathbf{v}_k \end{aligned} \tag{2}$$

where $\mathbf{w}_k \in \mathbb{R}^n$ is the process noise due to disturbances and modelling inaccuracies and $\mathbf{v}_k \in \mathbb{R}^l$ is the measurement noise due to sensor inaccuracy. They are both unmeasurable vector signals, but it is assumed that they are zero mean, stationary, Gaussian white noise processes.

Because SSI method has been theoretically developed for the excitation term being a zero-mean Gaussian white noise process, this method has been often perceived be to only valid for the ambient white noise testing procedure. However, when the input white noise process in SSI method is interpreted as ”system noise”, instead of ambient noise, SSI method is also theoretically applicable to the impact loading and step relaxation testing procedures.

1.4 Tests

Both tank and sea tests will be conducted for identifying the modal frequency and damping corresponding to the heave motion of the scaled star-spar buoy. In the tank test, a step relaxation testing procedure is to be followed, thus ERA will be the primary method to be used. For the sea test, the wave load acting on the tested buoy is difficult to measure, thus SSI will be utilized for estimating the modal frequency and damping. Since real wave excitation can be expressed as the output of a suitable filter excited with white noise input, some additional computational poles (frequencies and damping ratios) unrelated to the buoy may appear as a result of the white noise assumption.

Tank Test

The tank test of star-spar buoy was conducted in the acoustics tank of Middleton Building in the URI bay campus. The tank is 4 m wide, 7.6 m long, and 3.6 m deep. In the step relaxation test, the buoy was pulled upward to a certain height above its equilibrium position then released, and 60 sec of free decay heave acceleration data with a sampling rate 640 Hz were collected. Due to the small size of the tank, the measured response of the buoy would be affected by reflected waves. Thus, the measured response data are corrupted free response data. During the tank test, the LEG was fixed and would not oscillate under the buoy heave motion.

Sea Test

The sea test of the star-spar buoy was conducted in southwest of URI Narragansett Bay campus. The buoy was transported from the laboratory to the pier and deployed by a forklift jib crane into the water. It was then taken under tow by the R/V McMaster to the test location. A colocated spherical waverider buoy was concurrently deployed to measure the wave field in which buoy was operating. The star-spar buoy was instrumented to measure and record accelerometer data for buoy motion, electrical generator output, electrical generator position, generator loading, and charging circuit conditions. The buoy was released and allowed to heave and drift in an un-tethered fashion. During the test, the tide was ebbing with a mean current flow to the South. The wind was SSW at 10-15 knots. 3600 second of acceleration data with a sampling rate 64 Hz were collected. The LEG is free in the sea test and it oscillates as a result of buoy heave through coupled resonance.

1.5 Thesis Layout

This thesis consists of 5 chapters. Chapter 1 presents an introduction on the star-spar buoy under investigation, the deterministic and stochastic modal identification methods employed to estimate the modal properties of the star-spar buoy, and tank and field tests. Chapter 2 provides the mathematical background for those methods to be utilized in the following chapters, including Short Time Fourier Transform (STFT), Eigensystem Realization Algorithm (ERA) and Stochastic Subspace Identification (S-SI). Chapters 3 and 4 analyze the data collected from the tank and sea test, respectively. Because the interaction between buoy and surrounding fluid, the buoy-fluid system is a highly nonlinear system. It is a first approximation to treat this nonlinear system to be piecewise linear; consequently, a time-frequency analysis using short time Fourier transform will be conducted. It can be shown that a similar time-frequency analysis using ERA concept can also be performed. Both ERA and SSI methods will be implemented for estimating the modal frequency and damping ratio of the buoy-fluid system using tank and sea test data. Chapter 5 contains the conclusions of the presented work. Since the research in modal identification for buoy-fluid system is far from being well-studied, the major open problems are also listed.

CHAPTER 2

Preliminaries

This chapter provides the necessary mathematical background to conduct the signal analysis and modal identification for chapters 3 and 4. It includes a review of the short-time Fourier transform (STFT) for time-frequency signal analysis, Eigen-system realization algorithm (ERA) for deterministic system identification and stochastic subspace identification (SSI) for deterministic system identification, together with the introduction of Prony series for signal reconstruction.

2.1 Short Time Fourier Transform

Due to the fluid-structure interaction, the dynamics of any ocean buoy is likely to be nonlinear in nature. Thus, to analyze the frequency of the measured response signals of an ocean buoy is better to provide information on how the frequency changes over time. Among a number of time-frequency analysis techniques, the simplest and most popular one is the short-time Fourier transform (STFT) [8], which determines the sinusoidal frequency and phase content of local sections of a signal as it changes over time.

2.1.1 Continuous STFT

In the continuous-time case, the function to be transformed is simply multiplied by a window function which is nonzero for only a short period of time. The Fourier transform (a one-dimensional function) of the resulting signal is taken as the window is sliding along the time axis, resulting in a two-dimensional representation of the signal. Mathematically, this is written as:

$$\mathbf{STFT}(\tau, \omega) \equiv \mathrm{X}(\tau, \omega) = \int_{-\infty}^{\infty} x(t)\omega(t-\tau)e^{-j\omega t}dt \tag{3}$$

where $\omega(t)$ is the window function, and $x(t)$ is the signal to be transformed. $X(\tau, \omega)$ is essentially the Fourier Transform of $x(t)\omega(t-\tau)$, a complex function representing the phase and magnitude of the signal over time and frequency.

2.1.2 Discrete STFT

In the discrete time case, the data to be transformed could be broken up into chunks of frames. Each chunk is Fourier transformed, and the complex result is added to a matrix, which records magnitude and phase for each point in time and frequency. This can be expressed as:

$$\mathbf{STFT}x[n](m,\omega) \equiv \mathrm{X}(m,\omega) = \sum_{-\infty}^{\infty} x[n]\omega[n-m]e^{-j\omega n} \tag{4}$$

likewise, with signal $x[n]$ and window $\omega[n]$. In this case, m is discrete and ω is continuous, but in most typical applications the STFT is performed on a computer using the Fast Fourier Transform, so both variables are discrete and quantized.

2.2 Eigensystem Realization Algorithm

In the derivation of the Eigensystem realization algorithm, a time-invariant system is described by its state-space representation as [9]:

$$\begin{aligned} \dot{\mathbf{x}} &= \mathbf{A}_c\mathbf{x} + \mathbf{B}_c\mathbf{u} \\ \mathbf{y} &= \mathbf{C}\mathbf{x} \end{aligned} \tag{5}$$

where $\mathbf{x} \in \mathbb{R}^n$, $\mathbf{u} \in \mathbb{R}^m$ and $\mathbf{y} \in \mathbb{R}^l$ are the state, input, and output vectors, respectively; and n, m and l are the corresponding numbers of those vectors. The constant matrices $\mathbf{A}_c$, $\mathbf{B}_c$, $\mathbf{C}$ with appropriate dimensions represent the internal operation of the linear system.

The discrete-time version of the state-space representation is expressed as:

$$\begin{aligned} \mathbf{x}_{k+1} &= \mathbf{A}\mathbf{x}_k + \mathbf{B}\mathbf{u}_k \\ \mathbf{y}_k &= \mathbf{C}\mathbf{x}_k \end{aligned} \tag{6}$$

where k is the time index, and constant matrices $\mathbf{A}$ and $\mathbf{B}$ are derivable from $\mathbf{A}_c$ and $\mathbf{B}_c$. When a unit impulse excitation is taken for each input element, the results from Eq. 6

can be assembled into a pulse-response matrix $\mathbf{Y}_k \in \mathbb{R}^{m\times l}$ as follows:

$$\mathbf{Y}_1 = \mathbf{CB}, \;\; \mathbf{Y}_2 = \mathbf{CAB}, \cdots, \mathbf{Y}_k = \mathbf{CA}^{k-1}\mathbf{B} \tag{7}$$

The constant matrices in the sequence are known as Markov parameters. A system realization is the computation of a triplet $[\mathbf{A}, \mathbf{B}, \mathbf{C}]$ from the Markov parameters shown in Eq. 7, for which the discrete-time model, Eq. 6, is satisfied. Any system has an infinite number of realizations which will predict the identical response for any particular input, and a minimum realization means a model with the smallest state-space dimensions among all realizable systems that have the same input-output relations. The basic development of the state-space realization is attributed to Ho and Kalman [10] who introduced the important principles of minimum realization theory.

System realization begins by forming the generalized $\alpha l \times \beta m$ Hankel matrix, composed of the Markov parameters from Eq. 7:

$$\mathbf{H}(k-1) = \begin{bmatrix} \mathbf{Y}_k & \mathbf{Y}_{k+1} & \cdots & \mathbf{Y}_{k+\beta-1} \\ \mathbf{Y}_{k+1} & \mathbf{Y}_{k+2} & \cdots & \mathbf{Y}_{k+\beta} \\ \cdots & \cdots & \cdots & \cdots \\ \mathbf{Y}_{k+\alpha-1} & \mathbf{Y}_{k+\alpha} & \cdots & \mathbf{Y}_{k+\alpha+\beta-1} \end{bmatrix} \tag{8}$$

where α is the number of block rows in block Hankel matrix and β is the number of block columns. In contrast to classical system realization methods which use the generalized Hankel matrix given in Eq. 8, the ERA algorithm begins by forming an ERA block data matrix which is obtained by deleting some rows and columns of the generalized Hankel matrix of Eq. 8, but maintaining the first block matrix, $\mathbf{Y}_k$, intact. Furthermore, the standard ordering of entries in the generalized Hankel matrix does not need to be maintained. However, for the simplicity of presentation in this paper, we use the block Hankel matrix given in Eq. 8 as the ERA block data matrix.

After substituting the Markov parameters from Eq. 7 into Eq. 8, $\mathbf{H}(k-1)$ can be decomposed into three matrices:

$$\mathbf{H}(k-1) = \mathcal{P}_\alpha \mathbf{A}^{k-1} \mathcal{Q}_\beta \tag{9}$$

where the block matrix $\mathcal{P}_\alpha$ is the observability matrix

$$\mathcal{P}_\alpha = \begin{pmatrix} \mathbf{C} \\ \mathbf{CA} \\ \mathbf{CA}^2 \\ \cdots \\ \mathbf{CA}^{\alpha-1} \end{pmatrix} \in \mathbb{R}^{\alpha l \times n} \tag{10}$$

and the block matrix $\mathcal{Q}_\beta$ is the controllability matrix:

$$\mathcal{Q}_\beta = \left[\begin{array}{ccccc} \mathbf{B} & \mathbf{AB} & \mathbf{A}^2\mathbf{B} & \cdots & \mathbf{A}^{\beta-1}\mathbf{B} \end{array} \right] \in \mathbb{R}^{n \times \beta m} \tag{11}$$

In particular, substituting $k = 1$ and $k = 2$ into Eq. 9 yields

$$\mathbf{H}(0) = \mathcal{P}_\alpha \mathcal{Q}_\beta \tag{12}$$

and

$$\mathbf{H}(1) = \mathcal{P}_\alpha \mathbf{A} \mathcal{Q}_\beta \tag{13}$$

The ERA process starts with the factorization of $\mathbf{H}(0)$, which is obtained by replacing $k = 1$ in Eq. 8, using singular value decomposition [11],

$$\mathbf{H}(0) = \mathbf{USV}^T = \left[\begin{array}{cc} \mathbf{U}_1 & \mathbf{U}_2 \end{array} \right] \left[\begin{array}{cc} \mathbf{S}_1 & \mathbf{0} \\ \mathbf{0} & \mathbf{0} \end{array} \right] \left[\begin{array}{c} \mathbf{V}_1^T \\ \mathbf{V}_2^T \end{array} \right] \tag{14}$$

where the columns of matrices $\mathbf{U}$ and $\mathbf{V}$ are orthonormal and $\mathbf{U}_1$ and $\mathbf{V}_1$ are the matrices formed by the first n columns of $\mathbf{U}$ and $\mathbf{V}$, respectively; $\mathbf{S}_1 = \mathrm{diag}[\sigma_1, \sigma_2, \cdots, \sigma_n]$ with monotonically non-increasing σ_i, i.e. $\sigma_1 \geq \sigma_2 \geq \cdots \geq \sigma_n \geq 0$.

Comparison of Eqs. 12 and 14 suggests that $\mathcal{P}_\alpha$ is related to $\mathbf{U}_1$ and $\mathcal{Q}_\beta$ is related to $\mathbf{V}_1^T$. Indeed, one possible choice is $\mathcal{P}_\alpha = \mathbf{U}_1\mathbf{S}_1^{1/2}$ and $\mathcal{Q}_\beta = \mathbf{S}_1^{1/2}\mathbf{V}_1^T$. This choice appears to make both $\mathcal{P}_\alpha$ and $\mathcal{Q}_\beta$ balanced. With substituting these choices for $\mathcal{P}_\alpha$ and $\mathcal{Q}_\beta$ into Eq. 13, one obtains that

$$\mathbf{H}(1) = \mathcal{P}_\alpha \mathbf{A} \mathcal{Q}_\beta = \mathbf{U}_1\mathbf{S}_1^{1/2}\mathbf{A}\mathbf{S}_1^{1/2}\mathbf{V}_1^T \tag{15}$$

Premultipling $\mathbf{S}_1^{1/2}\mathbf{U}_1$ and postmultiplying $\mathbf{V}_1\mathbf{S}_1^{1/2}$ at Eq. 15 yields a minimum realization of $\mathbf{A}$ as

$$\hat{\mathbf{A}} = \mathbf{S}_1^{-1/2}\mathbf{U}_1^T\mathbf{H}(1)\mathbf{V}_1\mathbf{S}_1^{-1/2} \tag{16}$$

Here the quantities with "$\hat{\mathbf{A}}$" mean estimated quantities to distinguish from the true quantities.

From Eqs. 10 and 11, it is clear that the first m columns form the input matrix $\mathbf{B}$ whereas the first l rows form the output matrix $\mathbf{C}$.

2.2.1 Postprocessing

The realized discrete-time model represented by the matrices $[\hat{\mathbf{A}}, \hat{\mathbf{B}}, \hat{\mathbf{C}}]$ can be transformed to the continuous-time model. The system frequencies and dampings may then be computed from the eigenvalues of the estimated continuous-time state matrix.

Assuming that the state matrix $\mathbf{A}$ of order n has a complete set of linearly independent eigenvectors $\boldsymbol{\Psi} = [\boldsymbol{\psi}_1, \boldsymbol{\psi}_2, \cdots, \boldsymbol{\psi}_n]$ with corresponding eigenvalues $\boldsymbol{\Lambda} = diag(\lambda_1, \lambda_2, \cdots, \lambda_n)$ which are not necessarily distinct, we have

$$\mathbf{A}\boldsymbol{\Psi} = \boldsymbol{\Psi}\boldsymbol{\Lambda} \tag{17}$$

or

$$\boldsymbol{\Lambda} = \boldsymbol{\Psi}^{-1}\mathbf{A}\boldsymbol{\Psi} \tag{18}$$

The realization $[\mathbf{A}, \mathbf{B}, \mathbf{C}]$ can then be transformed to the realization $[\boldsymbol{\Lambda}, \boldsymbol{\psi}^{-1}\mathbf{B}, \mathbf{C}\boldsymbol{\psi}]$ in the *modal coordinates*. The diagonal matrix $\boldsymbol{\Lambda}$ contains the information of modal damping rates and damped natural frequencies. The matrix $\boldsymbol{\psi}^{-1}\mathbf{B}$ defines the initial modal amplitudes and the matrix $\mathbf{C}\boldsymbol{\psi}$ the mode shapes at the sensor points. All the modal parameters of a dynamic system can thus be identified by the triplet $[\boldsymbol{\Lambda}, \boldsymbol{\psi}^{-1}\mathbf{B}, \mathbf{C}\boldsymbol{\psi}]$.

Because of the relation

$$\mathbf{A} = \exp(\mathbf{A}_c \Delta t) \tag{19}$$

or

$$\boldsymbol{\Lambda} = \exp(\boldsymbol{\Lambda}_c \Delta t) \tag{20}$$

The desired modal damping rates and damped natural frequencies are simply the real and imaginary parts of the eigenvalues $\mathbf{\Lambda}_c$, after transformation from the discrete-time domain to the continuous-time domain using the relation $\mathbf{\Lambda}_c = \ln(\mathbf{\Lambda})/\triangle t$.

The values of $\mathbf{\Lambda}_c$ occur in complex conjugated pairs and can be written as

$$\lambda_{c_q}, \lambda_{c_q}^* = -\xi_q \omega_q \pm j\omega_q' \tag{21}$$

where ξ_q is the modal damping ratio of mode q, and ω_q, $\omega_q' = \omega_q\sqrt{1-\xi_q^2}$ are the undamped and damped eigenfrequencies of mode q (rad/s). Form the above equation, we have

$$\begin{aligned} \omega_q' &= \mathrm{Im}(\lambda_q) \\ \omega_q &= |\lambda_q| \\ \xi_q &= \frac{-\mathrm{Re}(\lambda_q)}{|\lambda_q|} \end{aligned} \tag{22}$$

In this section, it has been shown how the modal parameters could be extracted analytically from the identified system matrices $\mathbf{A}$ and $\mathbf{C}$.

2.3 Stochastic Subspace Identification

The stochastic subspace identification (SSI) method has been a proven method for a variety of engineering applications [12]. The detailed description of the SSI method is provided in [13], and a brief of the SSI method is presented below [14].

When no deterministic forces except the stochastic components (noise) are included, we have the following discrete-time stochastic state-space model for a dynamic system:

$$\begin{aligned} \mathbf{x}_{k+1} &= \mathbf{A}\mathbf{x}_k + \mathbf{w}_k \\ \mathbf{y}_k &= \mathbf{C}\mathbf{x}_k + \mathbf{v}_k \end{aligned} \tag{23}$$

where $\mathbf{A} \in \mathbb{R}^{n\times n}$ and $\mathbf{C} \in \mathbb{R}^{l\times n}$ are the system and measurement matrices, respectively; n is the number of state variables and l is the number of the output sensors; $\mathbf{w}_k \in \mathbb{R}^n$

is the process noise due to disturbances and modelling inaccuracies and $\mathbf{v}_k \in \mathbb{R}^l$ is the measurement noise due to sensor inaccuracy. They are both unmeasurable vector signals but we assume that they are zero mean, stationary, white noise vector sequences with covariance matrices:

$$\mathrm{E}\left[\begin{pmatrix} \mathbf{w}_p \\ \mathbf{v}_p \end{pmatrix} \begin{pmatrix} \mathbf{w}_q^T & \mathbf{v}_q^T \end{pmatrix}\right] = \begin{pmatrix} \mathbf{Q} & \mathbf{S} \\ \mathbf{S}^T & \mathbf{R} \end{pmatrix} \delta_{pq} \tag{24}$$

where E is the expected value operator and δ_{pq} is the Kronecker delta. The matrices $\mathbf{Q} \in \mathbb{R}^{n\times n}$, $\mathbf{S} \in \mathbb{R}^{n\times l}$ and $\mathbf{R} \in \mathbb{R}^{l\times l}$ are the auto- and cross-covariance matrices associated with the noise sequences $\mathbf{w}_k$ and $\mathbf{v}_k$.

In the first step of the SSI method, the output measurements $\mathbf{y}_k \in \mathbb{R}^l$ are gathered in a block Hankel matrix $\mathbf{H}$ with $2\,i$ block rows and j columns:

$$\mathbf{H} = \left(\begin{array}{cccc} \mathbf{y}_0 & \mathbf{y}_1 & \cdots & \mathbf{y}_{j-1} \\ \mathbf{y}_1 & \mathbf{y}_2 & \cdots & \mathbf{y}_j \\ \cdots & \cdots & \cdots & \cdots \\ \mathbf{y}_{i-1} & \mathbf{y}_i & \cdots & \mathbf{y}_{i+j-2} \\ \hline \mathbf{y}_i & \mathbf{y}_{i+1} & \cdots & \mathbf{y}_{i+j-1} \\ \mathbf{y}_{i+1} & \mathbf{y}_{i+2} & \cdots & \mathbf{y}_{i+j} \\ \cdots & \cdots & \cdots & \cdots \\ \mathbf{y}_{2i-1} & \mathbf{y}_{2i} & \cdots & \mathbf{y}_{2i+j-2} \end{array}\right) = \left(\frac{\mathbf{Y}_p}{\mathbf{Y}_f}\right) \tag{25}$$

where the time index $k = 0, \cdots, s$ and $s = 2i + j - 2$. The matrices $\mathbf{Y}_p$ and $\mathbf{Y}_f$ are defined by splitting $\mathbf{H}$ into two parts of i block rows, in which the subscripts p and f stand for past and future. The projection of the row space of future outputs into the row space of past outputs is defined as:

$$\mathscr{P}_i = \mathbf{Y}_f/\mathbf{Y}_p = \mathbf{Y}_f\mathbf{Y}_p^T(\mathbf{Y}_p\mathbf{Y}_p^T)^\dagger\mathbf{Y}_p \tag{26}$$

Numerically, a more effective way to obtain $\mathscr{P}_i$ is via the QR-factorization of $\mathbf{H}$, instead of implementing the above equation directly.

Applying the singular value decomposition of $\mathscr{P}_i$ yields:

$$\mathscr{P}_i = \begin{pmatrix} \mathbf{U}_1 & \mathbf{U}_2 \end{pmatrix} \begin{pmatrix} \mathbf{S}_1 & \mathbf{0} \\ \mathbf{0} & \mathbf{0} \end{pmatrix} \begin{pmatrix} \mathbf{V}_1^T \\ \mathbf{V}_2^T \end{pmatrix} = \mathbf{U}_1\mathbf{S}_1\mathbf{V}_1^T \tag{27}$$

The order of the system, n, is equal to the number of singular values in Eqn. (27) different from zero, i.e. rank($\mathscr{P}_i$) = n. We have $\mathbf{U}_1 \in \mathbb{R}^{li\times n}$, $\mathbf{S}_1 \in \mathbb{R}^{n\times n}$ and $\mathbf{V}_1 \in \mathbb{R}^{j\times n}$. For theoretical data, the singular values should go to zero when the rank of the matrix is exceeded. For measured data, however, due to random errors and small inconsistencies in the data, the singular values will not become zero but will become very small [15].

The main theorem of stochastic subspace identification states that the projection $\mathscr{P}_i$ is equal to the product of the observability matrix Γ_i and the Kalman filter state sequence $\hat{\mathbf{X}}_i$:

$$\mathscr{P}_i = \Gamma_i \hat{\mathbf{X}}_i \tag{28}$$

where the extended observability matrix Γ_i is

$$\Gamma_i = \begin{pmatrix} \mathbf{C} \\ \mathbf{CA} \\ \mathbf{CA}^2 \\ \cdots \\ \mathbf{CA}^{i-1} \end{pmatrix} \in \mathbb{R}^{li\times n} \tag{29}$$

and the forward Kalman filter state sequence

$$\hat{\mathbf{X}}_i = \begin{pmatrix} \hat{\mathbf{x}}_i & \hat{\mathbf{x}}_{i+1} & \cdots & \hat{\mathbf{x}}_{i+j-2} & \hat{\mathbf{x}}_{i+j-1} \end{pmatrix} \in \mathbb{R}^{n\times j} \tag{30}$$

This theorem can algebraically be summarized as follows: (1) rank of $\mathscr{P}_i$ = n, (2) row space of $\mathscr{P}_i$ = row space of Γ_i, and (3) column space of $\mathscr{P}_i$ = column space $\hat{\mathbf{X}}_i$. This summary is the essence of why the projection-based algorithm has been called a subspace algorithm: it retrieves system related matrices as subspaces of projected data matrices.

Our focus on using the SSI is to obtain realizations for system matrices $\mathbf{A}$ and $\mathbf{C}$, as the modal frequency, damping and mode shape, can be extracted analytically from the realized $\hat{\mathbf{A}}$ and $\hat{\mathbf{C}}$. While one possible way of obtaining Γ_i is

$$\Gamma_i = \mathbf{U}_1 \mathbf{S}_1^{1/2} \tag{31}$$

a possible realization $\hat{\mathbf{A}}$ can now be determined from the extended observability matrix by making use of the shift structure of the matrix Γ_i. Denote $\overline{\Gamma}_i$ as the extended observability matrix Γ_i without the first l rows, and $\underline{\Gamma}_i$ the extended observability matrix Γ_i without the last l rows. Observing Eqn. (29), we can easily show $\overline{\Gamma}_i = \underline{\Gamma}_i\mathbf{A}$, which suggests a possible realization being:

$$\hat{\mathbf{A}} = \underline{\Gamma}_i^{\dagger}\overline{\Gamma}_i \tag{32}$$

where "†" is the pseudo inverse operation. Furthermore, one possible realization for the measurement matrix $\hat{\mathbf{C}}$ can be obtained from the first l rows of Γ_i.

2.4 Using Prony Series for Signal Reconstruction

The so-called Prony series [16] is a linear combination of exponentials with real-valued and/or complex-valued exponents for the signal:

$$y(t) = \sum_{n=1}^{p} \gamma_n e^{\lambda_n t} \quad 0 \leq t \leq T \tag{33}$$

where p is the number of terms. In Eq. 33, because $y(t)$ is a real-valued signal, λ_n must either be real numbers or occur in complex conjugate pairs (not limited to be pure imaginary). Let $\lambda_n \equiv -\alpha_n + i\omega_n$, then α_n is the damping factor in seconds^{-1} and ω_n is the frequency in radians. The coefficients γ_n corresponding to complex exponents λ_n must also appear in complex conjugate pairs. Let $\gamma_n \equiv A_n \exp(i\theta_n)$, then A_n is the amplitude and θ_n is the sinusoidal initial phase in radians associated with $e^{\lambda_n t}$.

Eq. 33 is a continuous time series. In digital signal analysis, the continuous $y(t)$ is not known, and only equally spaced samples are available. Denoting sampling interval Δt, $t_k = k\Delta t$, and $y_k = y(t_k)$, where $k = 0, 1, ..., N-1$, we have the Prony series in discrete time as:

$$y_k = \sum_{n=1}^{p} \gamma_n z_n^k \tag{34}$$

where $z_n = e^{\lambda_n \Delta t}$.

In this study, once $z_n, n = 1, ..., p$, have been obtained by either ERA or SSI method, γ_n can be estimated by solving the matrix equation

$$\begin{pmatrix} z_1^0 & z_2^0 & \cdots & z_p^0 \\ z_1^1 & z_2^1 & \cdots & z_p^1 \\ \vdots & \vdots & \ddots & \vdots \\ z_1^{N-1} & z_2^{N-1} & \cdots & z_p^{N-1} \end{pmatrix} \begin{pmatrix} \gamma_1 \\ \gamma_2 \\ \vdots \\ \gamma_p \end{pmatrix} = \begin{pmatrix} y_0 \\ y_1 \\ \vdots \\ y_{N-1} \end{pmatrix} \tag{35}$$

in the least-squares sense. The matrix form given in Eq. 35 has been derived from repeatedly using Eq. 34. From γ_n, the corresponding amplitude and phase angle can then be calculated. After obtaining the frequency, damping ratio, initial amplitude and phase angle for each component, a reconstructed signal can be obtained by adding up all components.

CHAPTER 3

Tank Testing

3.1 Tank Experiment Set Up

The buoy under investigation is a self contained (water tight) multiple-spar buoy (Fig.2), in which the longer central spar is surrounded by shallower, satellite spars, providing both form stability and a reduced overall average draft of the system (necessary to achieve a proper heave resonance period). Inside of the longer central spar, a Linear Electric Generator (Fig.3) is housed and suspended and has a massive ballast simply suspended to the bottom of its magnetic armature.

2. Star-spar buoy model

3. LEG model.

While conducting the laboratory and field testing, three three-axis (WIFI) accelerometers were mounted within the buoy models: one measured the central spar and another two measured satellite spars motions. For this thesis, however, only the heave motion data from the central spar is utilized for analysis.

In the tank test, the buoy is released from an initial position which is upwards from its equilibrium position in still water. Under an ideal situation, the buoy would undergo a clean damped free oscillation. However, due to the small size of the testing tank($4m \times 7.6m \times 3.6m$), the measured response signal would be contaminated by the reflected waves. A 60-sec of acceleration data, with sampling rate 640 Hz, is shown in Fig. 4. The signal seems to exhibit the beating phenomenon which might be caused by the summation of components with close frequencies.

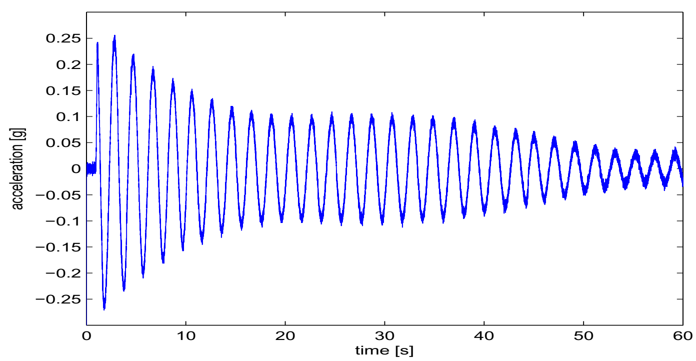

Figure 4. Tank Test Data

3.2 Short Time Fourier Transform Analysis

A plot of the STFT of the signal presented in Fig. 4 is shown in Fig.5, which has been obtained by using a sliding window with length 10 s (thus the frequency resolution is 0.1 Hz), and the sliding distance (time resolution) 0.1 s. The image of the STFT is not only limited by its frequency resolution, but also suffers the leakage problem inherited from using discrete Fourier transform (DFT). The effect of leakage suggests also that the peak amplitude associated with the STFT image is most likely smaller than the corresponding true amplitude.

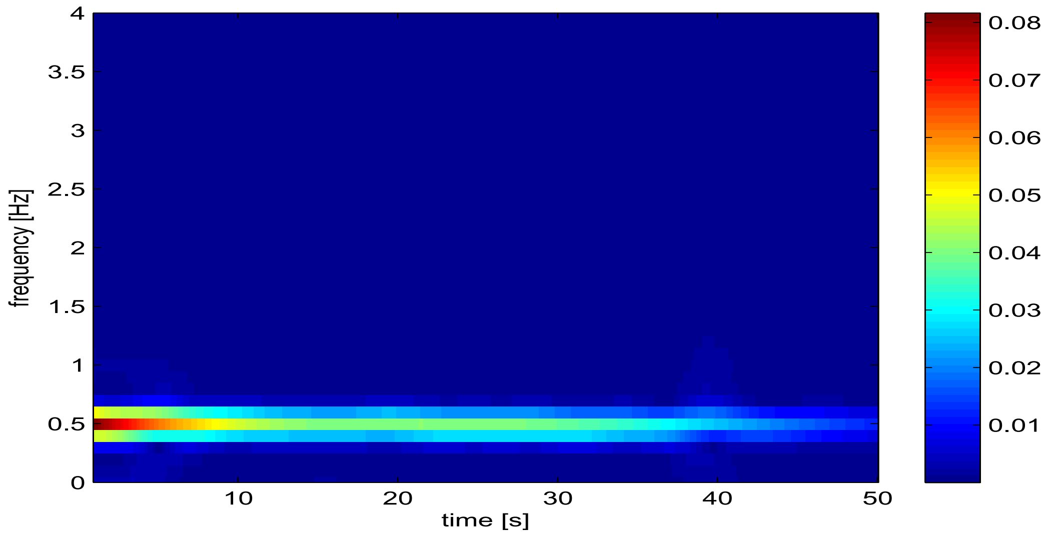

Figure 5. Short Time Fourier Transform of Tank Test Data

3.3 Tank Test Data Analysis by ERA

3.3.1 System Identification

While carrying out the eigensystem realization algorithm for the tank data, the Hankel matrix has been chosen close to a square matrix for the purpose of rejecting much noise in the modal identification. Determining the model order (or number of modes) that have contributed to the analyzed acceleration signal is by estimating the rank of the chosen Hankel matrix. For a response signal contributed only by M modes, the rank of the Hankel matrix should be $2M$, which is twice the number of modes contained to the signal. Estimating the rank of a matrix (based on a chosen singular value threshold) could be done if the singular values of the matrix have been ordered sequentially from the largest to the smallest. A conventional way to choose the noise threshold is to find a significant gap of the normalized singular values, but the choice of the noise threshold is always subjective because the weak signals and noise components are hard to separate. The normalized singular value diagram in Fig. 6 indicates that the measured signal might have one dominant component (at rank=2), one weak component (at rank=4), and one very weak component (at rank=6), together with much noise. Table.1 lists the estimated frequency and damping ratio from the tank test data by ERA when the model order is chosen equal to 2, 4 and 6, respectively.

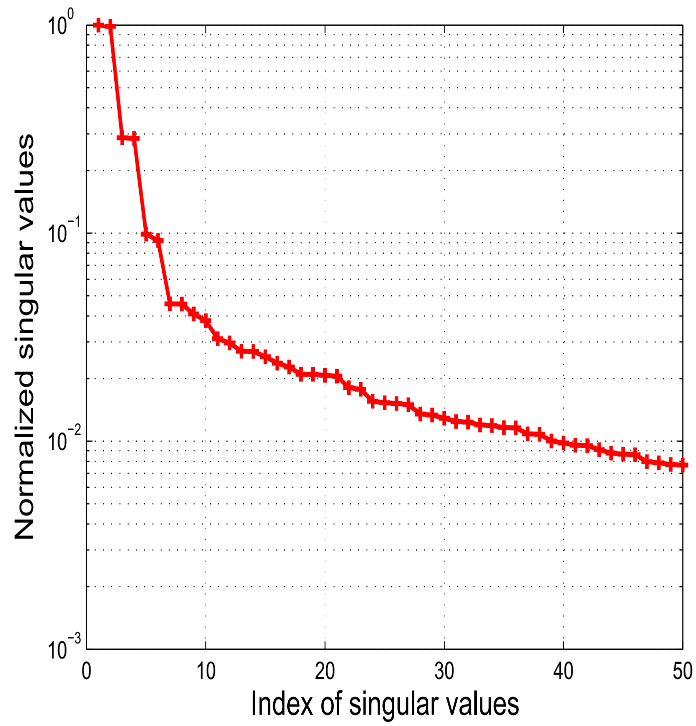

Figure 6. Normalized Singular Value Diagram of Tank Data by ERA

Table 1. Estimated frequency and damping ratio from the tank test data by ERA

Model Order	Frequency (Hz)	Damping ratio
2	0.4971	0.0257
4	0.4983	0.0691
	0.4830	0.0282
6	0.4619	0.0120
	0.4901	0.0245
	0.5021	0.1523

Often a better way to identify all poles should be through the combined usage of a stabilization diagram though. The stability diagram shown in Fig.7 is obtained from implementing ERA method by selecting the model orders ranged from 2 to 30, in which poles are labeled as stable when they are within the limitations of 1% difference for frequency and 5% for damping ratio among two consecutive model orders, namely:

$$\frac{|f^{(n)} - f^{(n+1)}|}{f^{(n)}} < 1\% \qquad \frac{|\xi^{(n)} - \xi^{(n+1)}|}{\xi^{(n)}} < 5\%$$

where $f^{(n)}$ and $\xi^{(n)}$ denote an estimated frequency and damping ratio with model order n. Throughout this study, the same stability criteria are applied to all stability diagrams. Fig.7 suggests that increasing the model order would not result in a better modal identification. When the model is taken equal to 4, two close frequencies are estimated to be about 0.49 and 0.48 Hz. The blue curve in the background of stability diagram is the DFT of the signal.

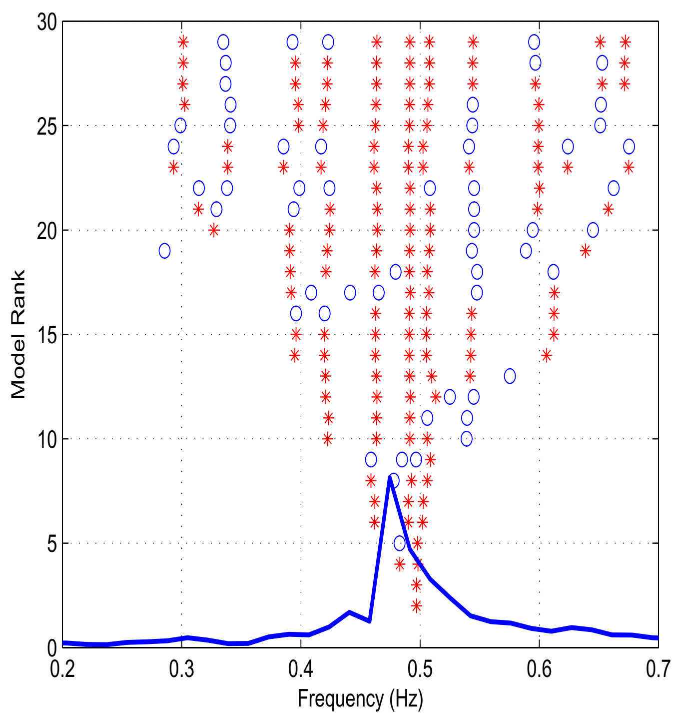

Figure 7. Stability Diagram of Tank Data by ERA

3.3.2 Time-Frequency Domain Analysis

The underlying assumption of ERA is that the dynamic system must be linear, but the buoy-fluid system is most likely to be highly nonlinear. Using the concept of a sliding window is to assume that the system is linear within the adopted window length. Clearly, the sliding window should be small enough to ensure that the system is approximately linear within the window length, but should be big enough to have enough data to reliably estimate the system frequencies and damping ratios. Larger windows also result in increased temporal smoothing. In any statistical undertaking, there is usually some trade-off between accuracy and reliability. Generally, any increase in accuracy comes at the expense of reliability.

With the sliding windows having length equal to 2s, 4s and 6s, and sliding distance 0.078125 s, Figs. 8(a) and 8(b) show the difference of estimated frequency and damping ratio, respectively. Notice that the curves corresponding to the 2s window exhibit much larger fluctuation in the estimated frequency and damping ratio. When the window length increases, the corresponding curves for the estimated frequency and damping ratio become smoother. As to be demonstrated later in the signal reconstruction, a segment of 6 s reconstruction can match well with the measured segment. Thus, a reasonable window length could be 6 s, since it reduces the undesirable fluctuation while still preserving some of the temporal dynamics of interest. As the fluctuation of the damping ratio is much higher than that of the frequency, this suggests that the estimated damping ratio is less reliable than the estimated frequency.

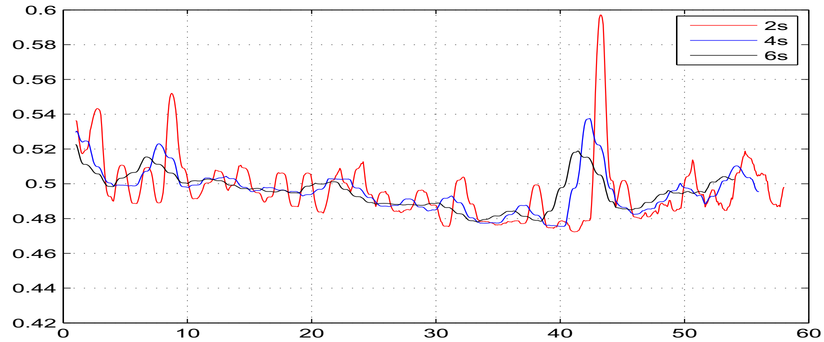

(a) Comparison the time series of natural frequency between different sliding window

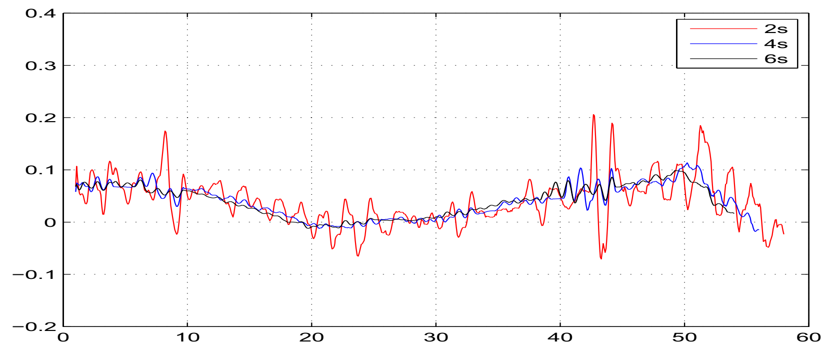

(b) Comparison the time series of damping ratio between different sliding window

Figure 8. Testing the Influence of the Window Size using Tank Test Data by ERA

Time-frequency Image plots for amplitude and damping

Fig. 8(a) shows the variation of the estimated frequency over time, but it does not provide the information about the corresponding amplitude of the component. Similar to the STFT image plot, Fig.9 presents the amplitude image while using ERA with the model order set equal to 10. The color intensity in the plot represents the initial amplitude of each damped components. Whereas the signal contains energy over a range of frequencies up to 3 Hz, the dominant frequency component is close to 0.5 Hz. Fig.10 is a enlarged plot Fig.9, with the frequency range of interest from 0.45Hz to 0.55Hz.

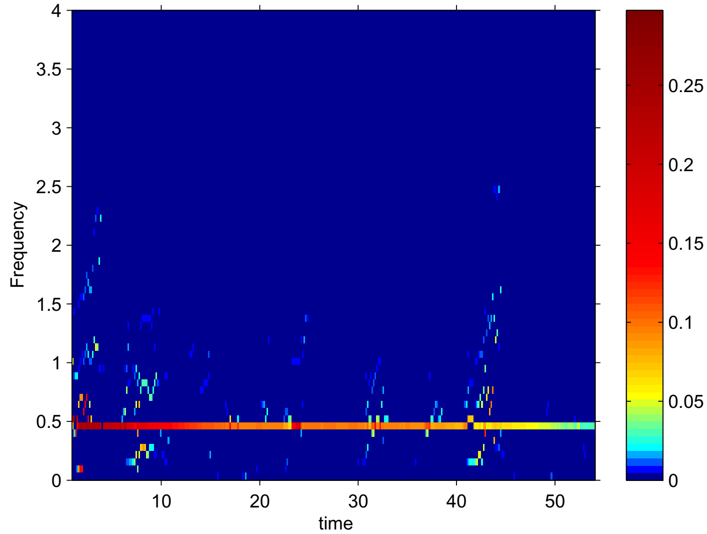

Figure 9. Time series of amplitude image (model order=10) of tank test by ERA

Shown in Fig.11 is the amplitude image for the frequency range from 0.45Hz to 0.55Hz when the model order is set equal to 2. A direct comparison between Fig. 10 (for model order equal to 10) and Fig. 11 (for model order equal to 2) suggests that they have very similar variation of the estimated frequency over time, but Fig. 11 corresponding to a lower model order exhibits a smoother variation than Fig. 10. The significant variation of the estimated modal frequency over time also suggests that either the buoy-fluid system is nonlinear or the free oscillation response has been contaminated by reflected waves, or both.

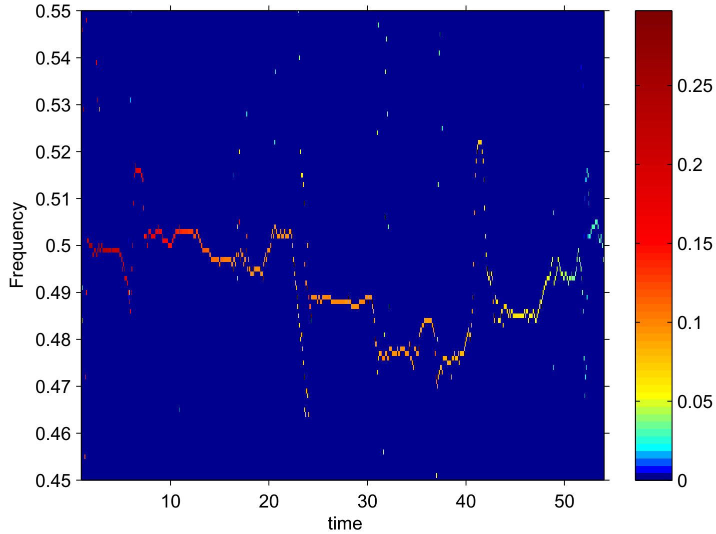

Figure 10. Zoom in the time series of amplitude image (model order=10) of tank test by ERA

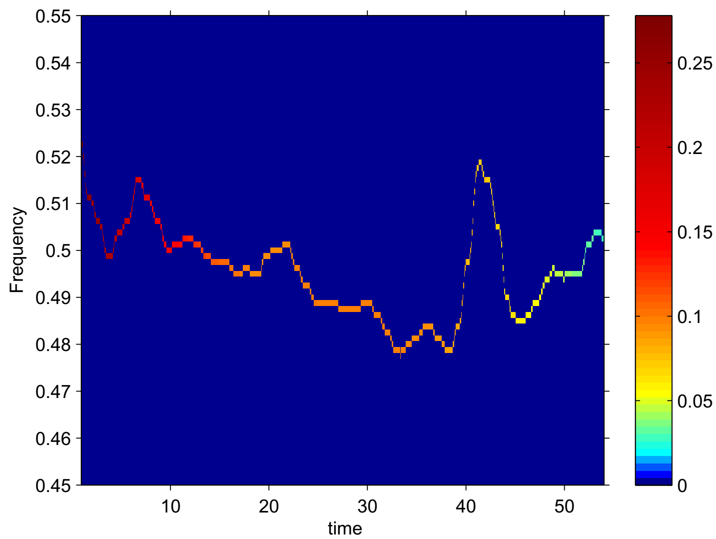

Figure 11. Time series of amplitude image (model order=2) of tank test by ERA

For completeness, Fig.12 shows the estimated damping image for the frequency range from 0.45Hz to 0.55Hz when the model order is set equal to 2. It is difficult to explain in physics why a negative damping occurs at the time around 20 s, but the signal shown in Fig. 4 certainly indicates that a negative damping (i.e. signal grows in amplitude over time) is possible at the time around 20 s.

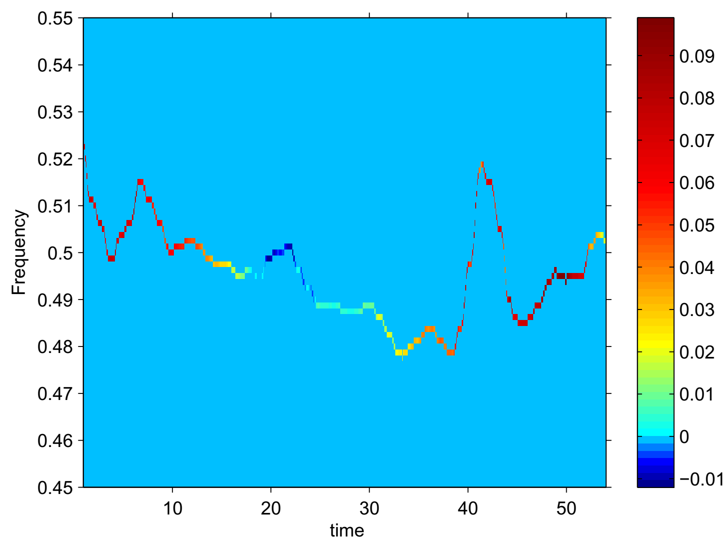

Figure 12. Time series of damping image (model order=2) of tank test by ERA

3.3.3 Signal Reconstruction using ERA estimates

Fig.13(a) through Fig.13(d) display 4 reconstructed signals, together with the measured signal, generated by using Prony series (see Eq. 34) with the component parameters estimated by using ERA with model order set equal to 2. These 4 reconstructed signals are based on window sizes equal to 1, 2, 4 and 6 seconds, respectively. The results suggest that the reconstruction of a 6-second signal can still match the original signal well.

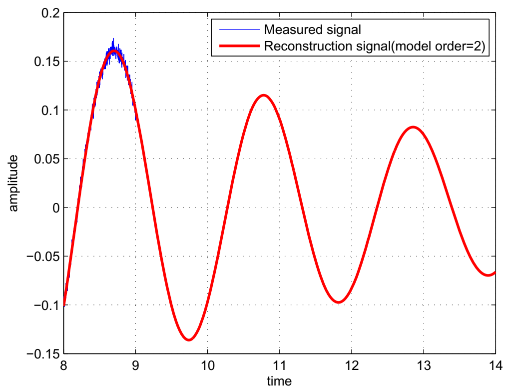

(a) One Second

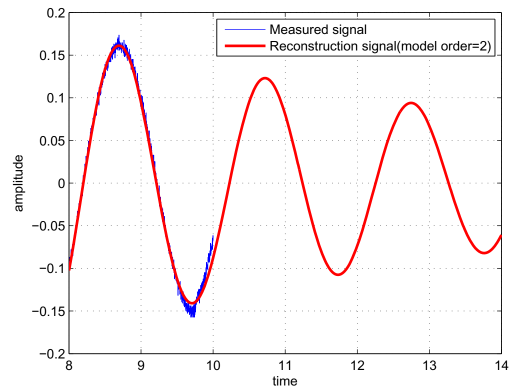

(b) Two Second

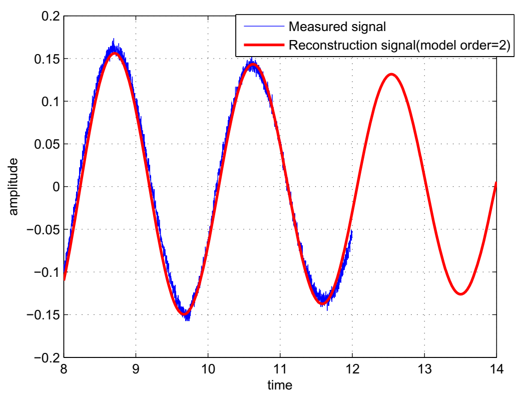

(c) Four Second

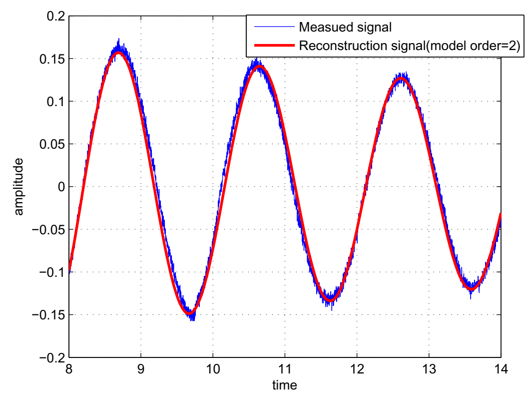

(d) Six Second

Figure 13. Comparison of reconstruction from different length of data by ERA

For a 6-second window, we also investigate the influence of the model order on the curve fitting of the reconstructed signals. In Fig.14, the green and red curves are based on model order equal to 10 and 2, respectively. Clearly, the curve fitting based on model order 10 is much better than that model order 2. The black curve in Fig.14 is the dominant component of the reconstructed signal with model order 10. Although the measured signal is mainly contributed by this dominant component (black curve), the fitting of the black curve (to the measured signal) is not as good as that of the red curve.

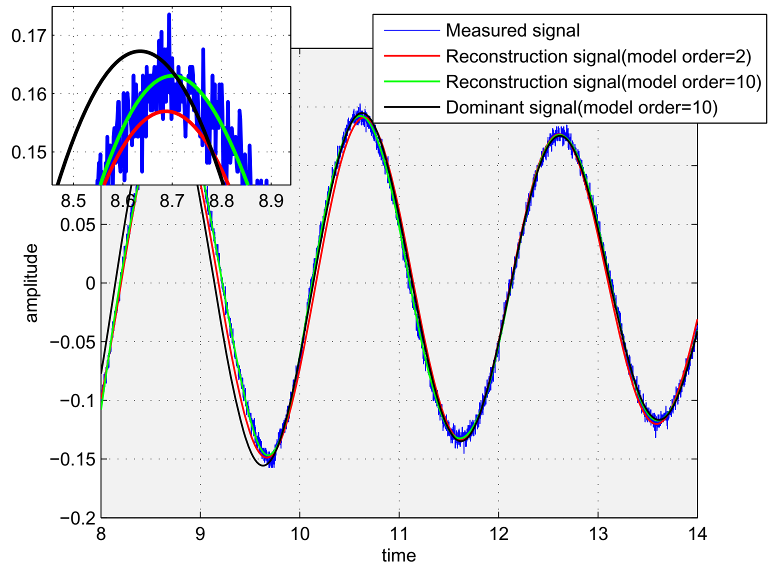

Figure 14. Comparison of the reconstruction signal by ERA from tank data(6s)

3.4 Tank Test Data Analysis by SSI

3.4.1 System Identification

While implementing SSI-data method, an issue is related to the dimension of the Hankel matrix $\mathbf{H}$, i.e. i and j in Eq. 32 , produced from the measured signal. When $\mathbf{H}$ is closer to a square matrix, it is more time consuming to perform the QR-factorization of $\mathbf{H}$ and the SVD of $\mathscr{P}_i$, and produces more number of singular values. On the other hand, When $2i << j$, performing the SVD of $\mathscr{P}_i$ is more computationally efficient, but might yield the model order too low to absorb signal noise. In this study, a Hankel matrix with $i = 100$ has been employed. The selection of $i = 100$ has not been completely arbitrary, but a choice according to prior evaluation on various selections of i and j.

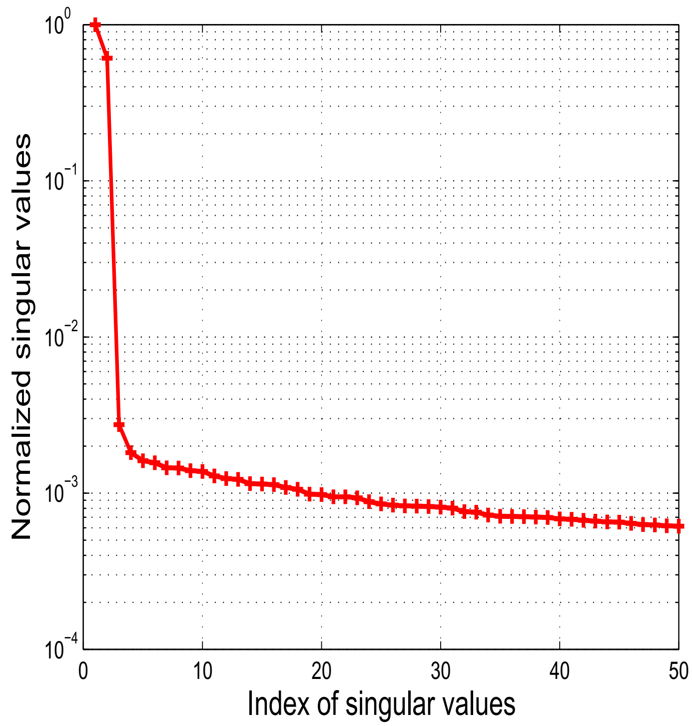

Figure 15. Normalized Singular Value Diagram of Tank Data by SSI

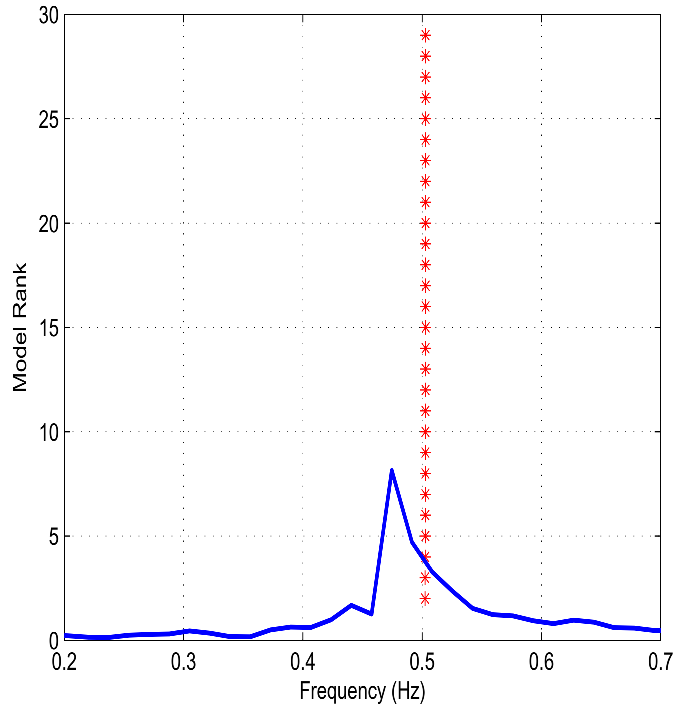

Figure 16. Stability Diagram of Tank Data by SSI

Fig.15 and Fig.16 show the normalized singular value diagram and stabilization diagram, respectively. From Fig.15, it suggests that just one system pole would be extracted from the measured signal. Clearly, Fig. 16 by SSI method gives a much cleaner stabilization diagram than Fig.7 by ERA method. When the model order is set equal to 2, the modal frequency and damping estimated by SSI method are 0.5025 Hz and 0.0581, respectively.

3.4.2 Time-Frequency Domain Analysis

Similar to Fig. 8(a) and Fig.8(b) by using ERA, Fig.17(a) and Fig.17(b) by using SSI show the the difference of the estimated frequency and damping ratio, respectively, when the sliding windows are taken equal to 2s, 4s and 6s, with sliding distance

0.078125 sec. As expected, when the window size is larger, the estimated curve will become smoother.

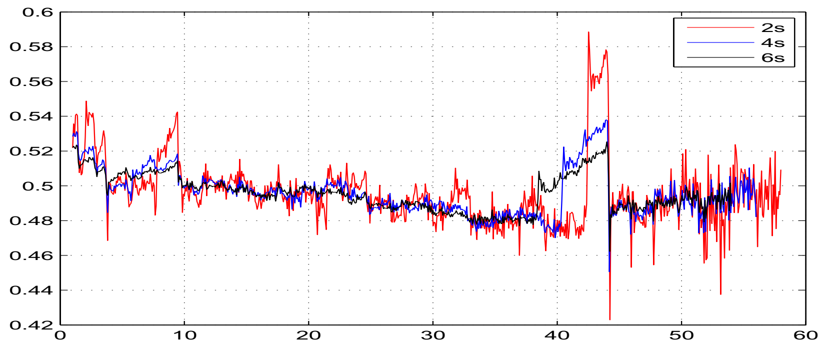

(a) Time series of frequency comparison

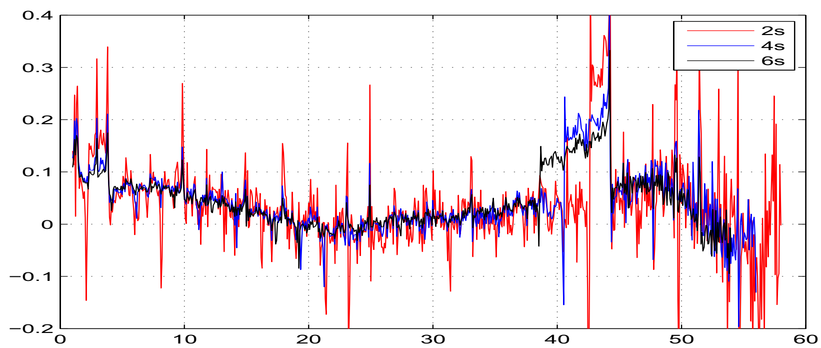

(b) Time series of damping comparison

Figure 17. Testing the Influence of window size using Tank data by SSI

Image of Amplitude and Damping

Fig. 18 for SSI is the counterpart of Fig. 9 for ERA, when the model order has been set equal to 10. The observation that Fig. 18 is much cleaner than Fig. 9 is not surprising at all because just one system pole would be extracted from the measured signal while using SSI method (see Fig.15). Furthermore, a zoom-in image from Fig. 18 is shown in Fig.19 where the frequency range is from 0.45Hz to 0.55Hz. When the model order has been set equal to 2, a similar image to Fig. 19 is shown in Fig. 20. Overall, the difference between them is not much.

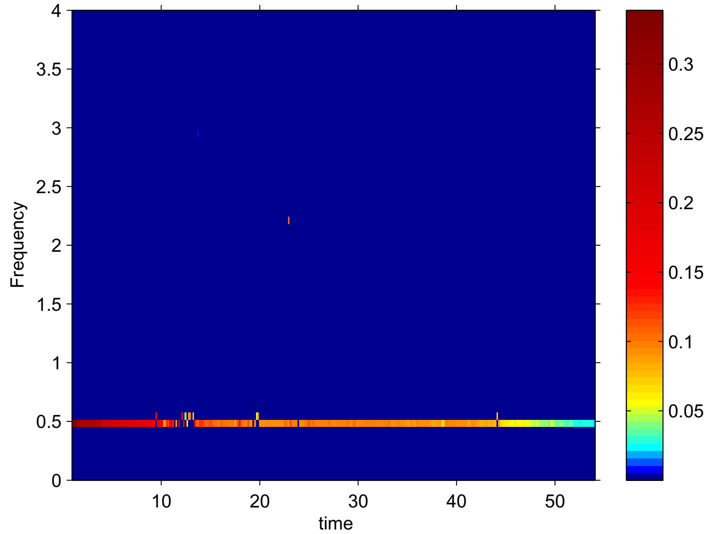

Figure 18. Time series of amplitude image (model order=10) of tank test by SSI

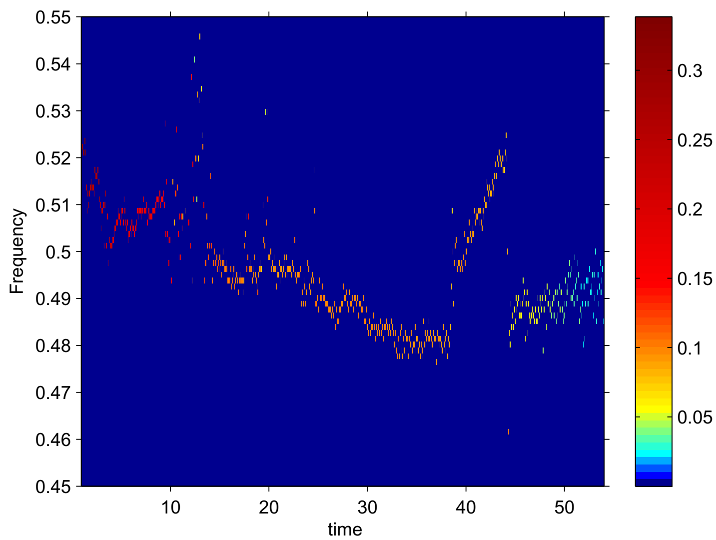

Figure 19. Time series of zoom in amplitude image (model order=10) of tank test by SSI

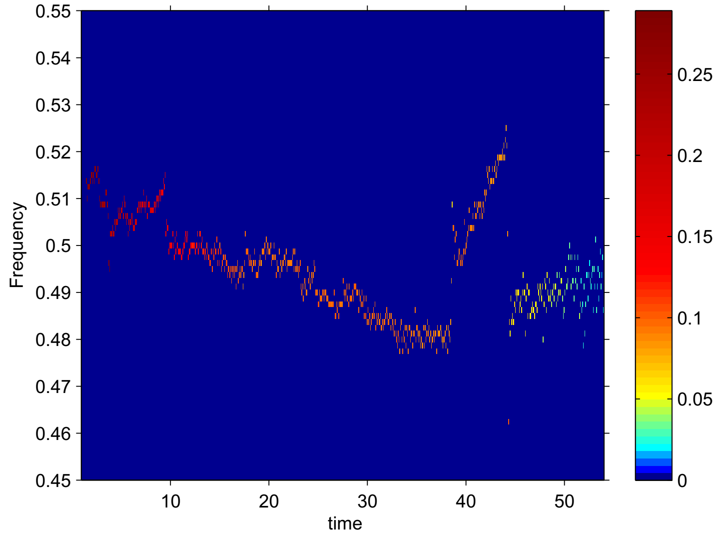

Figure 20. Time series of amplitude image (model order=2) of tank test by SSI

Fig. 21 shows the damping image when the model order is equal to 2, and it agrees with Fig. 12 (by ERA) that negative damping occurs at the time around 20 s.

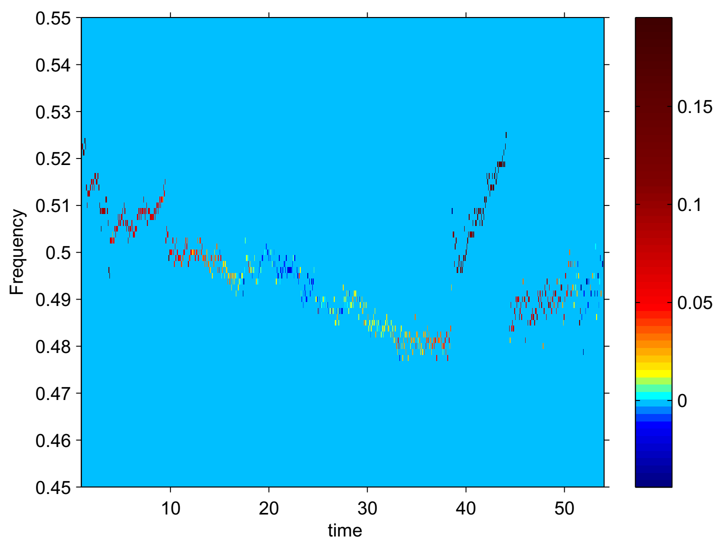

Figure 21. Time series of damping image (model order=2) of tank test by SSI

3.4.3 Signal Reconstruction using SSI estimates

Fig.22(a) through Fig.22(d), produced by the same way as Fig.13(a) through Fig.13(d) except with the component parameters estimated by using SSI, suggest that the reconstruction of a 6-second signal can still reasonably match the original signal.

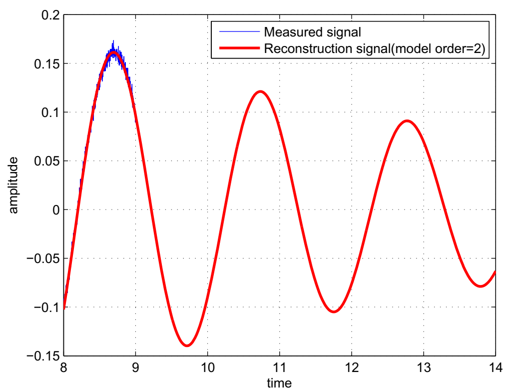

(a) One Second

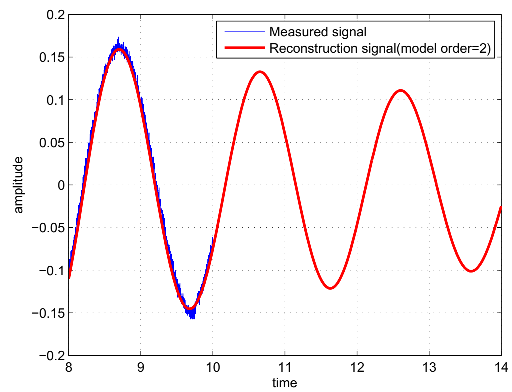

(b) Two Second

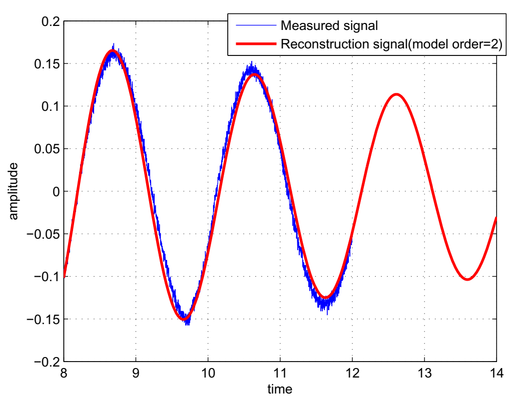

(c) Four Second

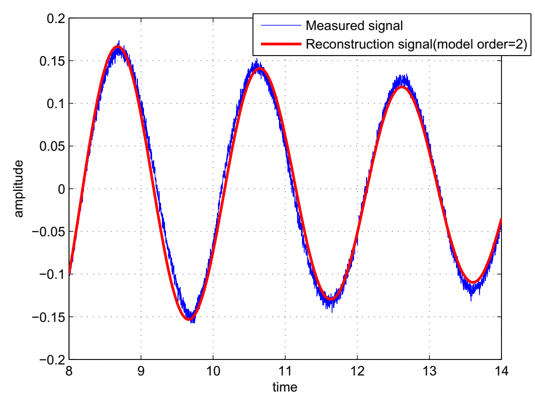

(d) Six Second

Figure 22. Comparison of reconstruction from different length of data by SSI

In a 6-second reconstruction, the green and red curves at Fig.23 are based on model order equal to 10 and 2, respectively. The difference between these two curves is insignificant, and neither curve matches the measured signal as good as the ERA curve based on model order 10 (the green curve in Fig.14).

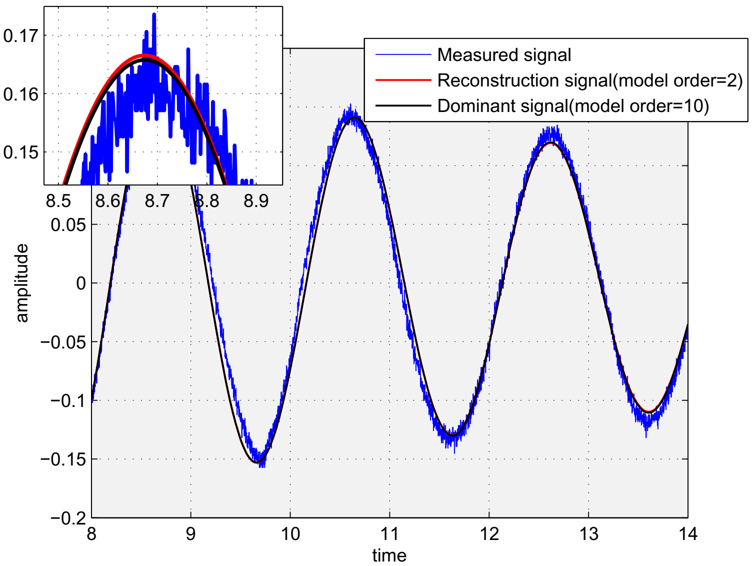

Figure 23. Comparison of the reconstruction signal by SSI from tank data(6s) of tank test by SSI

3.5 Summary and Discussion

The discrete Fourier transform of a signal can be viewed as a signal decomposition technique which decomposes a “periodic” signal into many harmonic components. Sequentially, picking the peaks from the Fourier frequency spectrum has also been employed as a simple “modal identification” technique. However, the concept of modal identification should not be confused with that of the signal decomposition. While the performance of a signal decomposition technique can be judged based on the fitting between the reconstructed signal and the original signal, that of a system identification technique can be judged based on the evaluation of stabilization diagram if no true solution is available.

Although ERA has long been perceived to be an effective modal identification technique for dealing with free oscillation signal, it was found that ERA is not the best modal identification technique if the free oscillation signal has been contaminated. In dealing with the distorted free oscillation signal measured from a small tank, where the measured free oscillation signal would be affected by reflected waves, it was found that SSI outperforms ERA for modal identification. While the stabilization diagram associated with SSI exhibits one clean and stable pole, that associated with ERA does not. While analyzing the whole 60-second response signal of the star-spar buoy, the estimated modal frequency is 0.4971 Hz by ERA, and 0.5025 Hz by SSI when the model order has been preset equal to 2. The corresponding damping ratios are 0.0257 and 0.0581, respectively. The agreement between ERA and SSI on the estimated modal frequency is excellent, and that on the estimated damping ratio seems also reasonable in view of the facts that the buoy-fluid system is nonlinear and that the free oscillation data has been polluted by reflected waves.

The numerical study in this chapter also demonstrates that using ERA to estimate component frequencies and damping ratios, together with a least-squares solution for getting amplitudes and phase angels, is an excellent signal decomposition technique. Whereas the time-frequency analysis by employing STFT is often limited by the frequency resolution and suffers the frequency leakage problem, that by using ERA can overcome both frequency resolution and leakage issues.

CHAPTER 4

Sea Testing

4.1 Sea Experiment Set Up

The sea test of the star-spar buoy was conducted on July 2010 in Narragansett Bay, RI. The buoy was taken under tow to the test location, then released and allowed to heave and drift in an un-tethered fashion. A co-located spherical "waverider" buoy was concurrently deployed to measure the wave field in which the buoy was operating. The test location and ship track (in proximity to the buoy's) is shown in Fig.24.

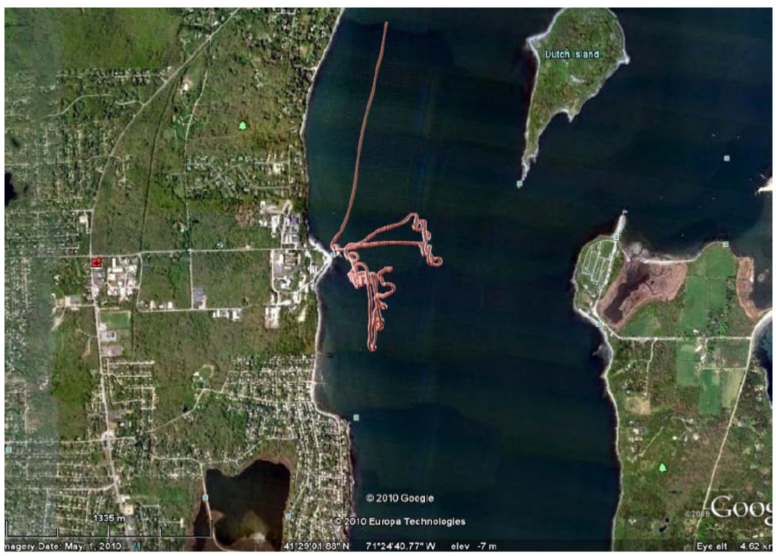

Figure 24. Test Location and Boat Track of the Sea Test

During the test, the tide was ebbing with a mean current flow to the South. The wind was SSW at 10-15 knots. For the present study, a 3600-second acceleration data (see Fig. 25) with a sampling rate 64 Hz will be utilized. It was noticed that several sharp "spikes" are evident that occur concurrently on all data channels. The sharp spike in the signal Fig. 25 is not noise, but is in fact, the mass-spring oscillator driving the LEG reaching the maximum extent of its displacement and slamming into the top and bottom of its support structure. This impulsive acceleration vibrates the entire structure and is detectable on all other data channels, including the satellite spars. This phenomenon also represents energy that is lost to extraction.

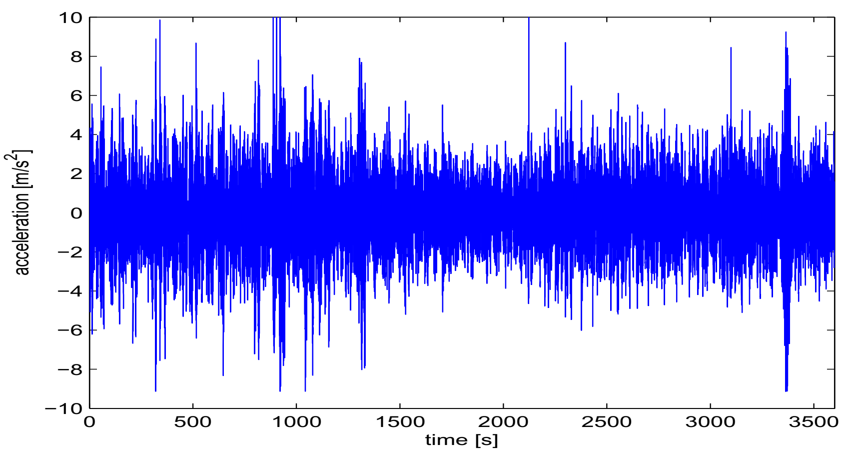

Figure 25. Sea test data

4.2 Short Time Fourier Transform Analysis

Fig.26(a) and Fig.26(b) are the image plots of the STFT of the sea test data, using a 50-second sliding window and sliding distance 1 second each time. Due to the 50-second sliding window, the frequency resolution has been limited to 0.02 Hz [i.e., 1/(window size in seconds)], and the Nyquist frequency is 32 Hz (a half of the sampling frequency). These image plots indicate that most energy of the response signal is around 0.5 Hz.

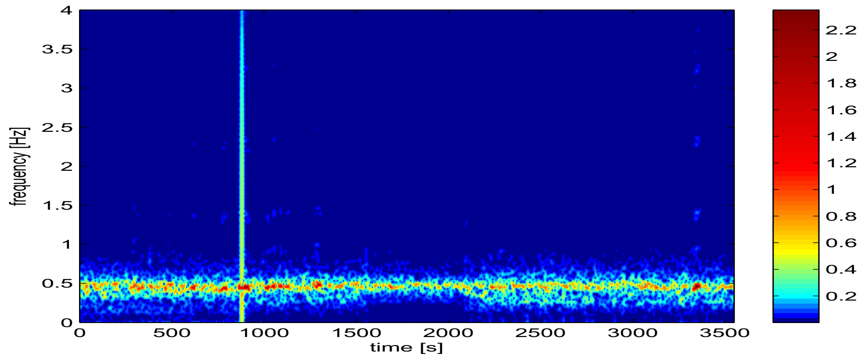

(a) Spectrum of STFT

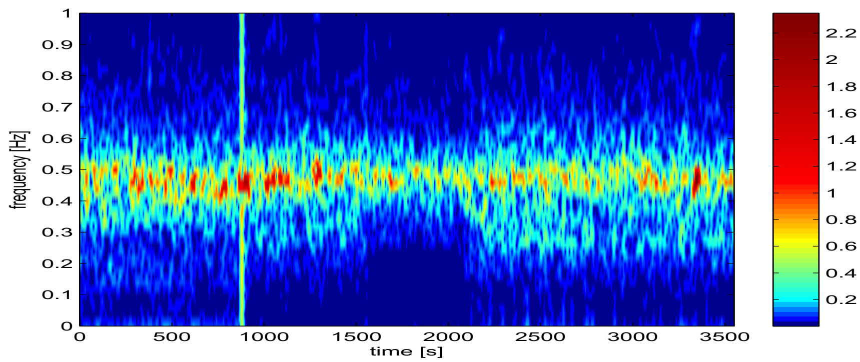

(b) Zoom in of Spectrum of STFT

Figure 26. Spectrum of STFT for sea test data

4.3 Sea Test Data Analysis by ERA

4.3.1 System Identification

Only the first 300 seconds of the above sea test signal is analyzed while implementing ERA, and the normalized singular value diagram computed from the corresponding square Hankel matrix associated with the 300-second signal is presented in Fig.27. From this figure, we conclude that the 300-second signal has only one major damped harmonic component, and a subjective noise threshold could be set at rank equal to 14 (i.e., 7 signal components). The stabilization diagram of using ERA for the 300-second signal is shown in Fig.28, where 7 stable poles are clear, all with frequency between 0.4 and 0.52 Hz. Obviously, the discrete Fourier spectrum (see the background curve) can not identify those 7 poles.

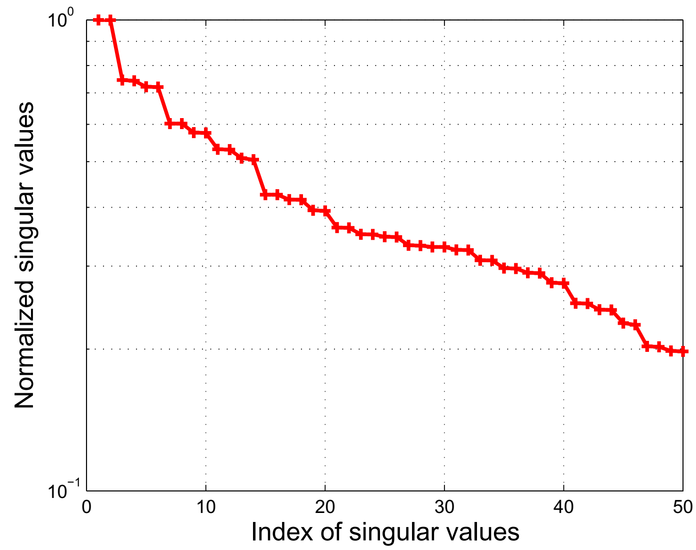

Figure 27. Normalized Singular Value Diagram of sea test data (0∼300s) by ERA

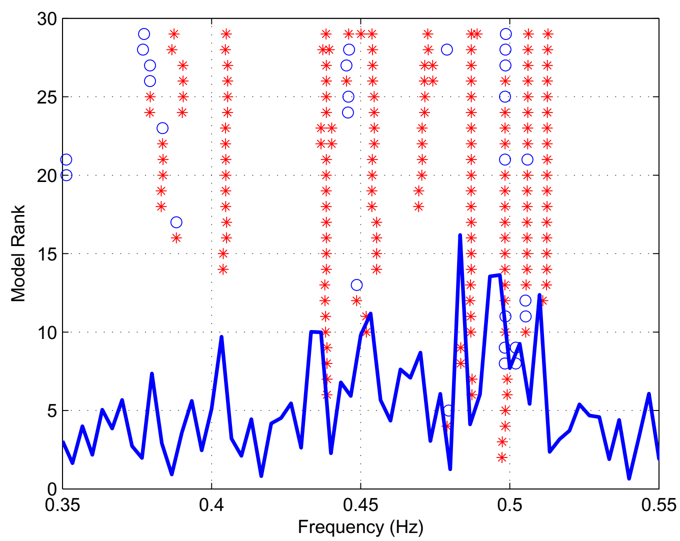

Figure 28. Stability Diagram of sea test data (0∼300s) by ERA

4.3.2 Signal Reconstruction

The part of signal from 135 to 175 second is taken to demonstrate the performance of signal decomposition and reconstruction by using ERA. Observing the singular value diagram (Fig. 29) and the stabilization diagram (Fig. 30) suggests that there are 3 or 5 significant components. To have a better reconstruction, many more components are necessary.

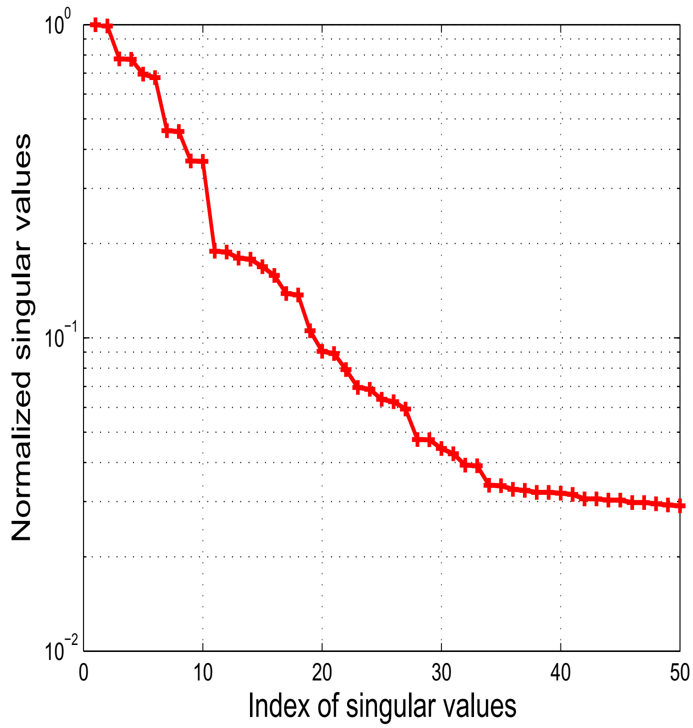

Figure 29. Normalized Singular Value Diagram of sea test data (135∼175s) by ERA

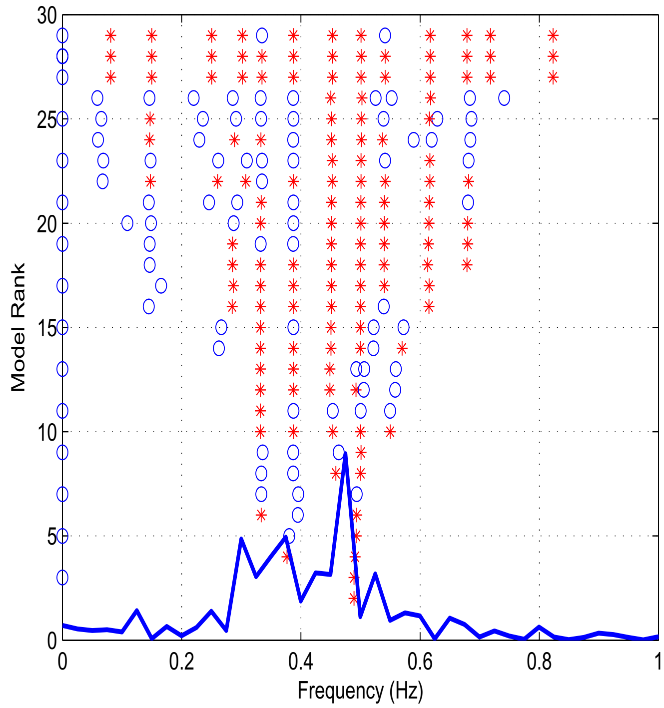

Figure 30. Stability Diagram of sea test data (135∼175s) by ERA

Shown in Figs. 31(a) through 31(d) are the reconstructed signals based on the first 3, 5, 9 and 16 components, respectively. Indeed, the first 3 components are most significant to the reconstruction of the signal. When the first 16 components are included, it can almost fully recover the measured signal.

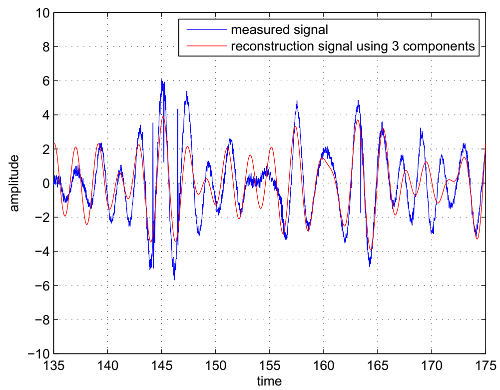

(a) 3 components

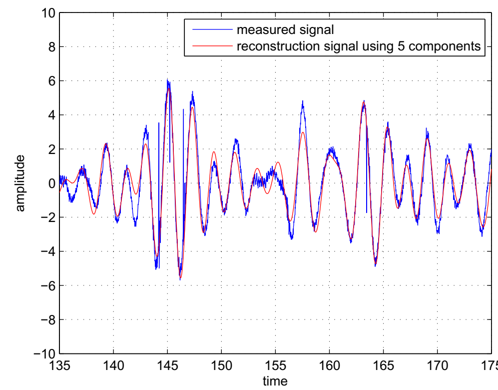

(b) 5 components

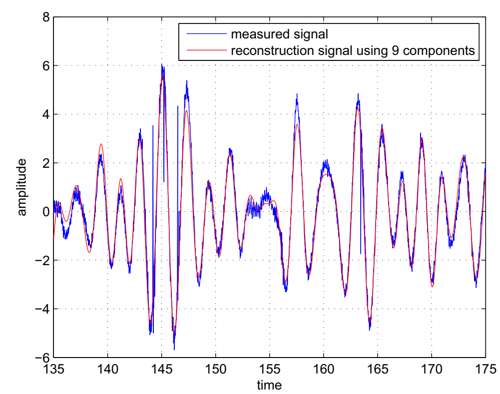

(c) 9 components

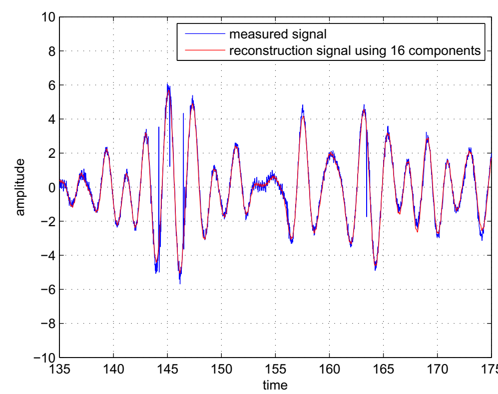

(d) 16 components

Figure 31. Comparison of the reconstruction signals by using various numbers of components

4.3.3 Time-Frequency Domain Analysis

While using ERA with the model order set equal to 20, Fig. 32 displays the amplitude image for the time-frequency analysis, where the amplitude intensity is the initial amplitude of each damped components. For the first 300 seconds of the sea test signal, it contains components mainly having frequencies between 0.1 and 0.7 Hz, and most dominant components between 0.4 and 0.5 Hz. This image plot is a significant improvement over that of using STFT.

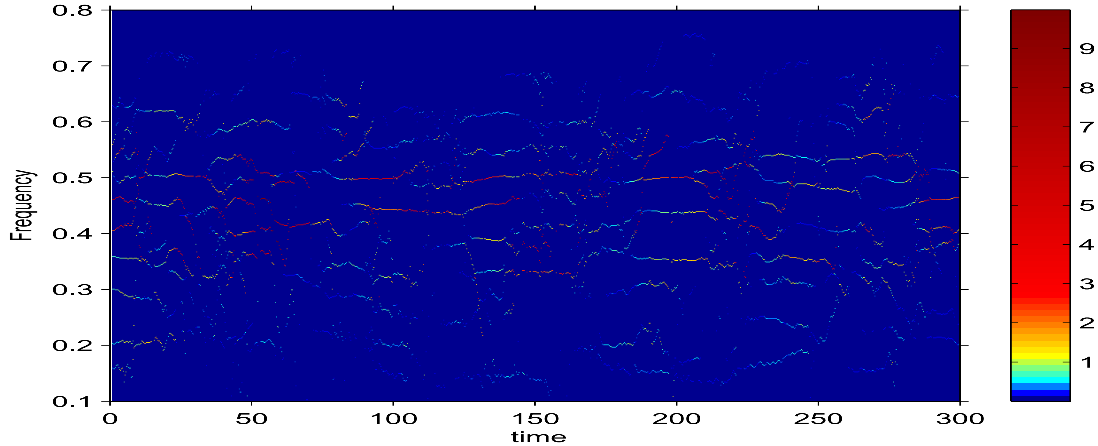

Figure 32. Amplitude image of time-frequency analysis using sea test data (0 $\sim$ 300s) by ERA

4.4 Sea Test Data Analysis by SSI

4.4.1 System Identification

Let the 3600-second sea test data be divided into 4 equal-length segments: 900 seconds for each segment. In this section, each 900-second segment is treated as an independent test, and the results of modal identification from these four segments are compared against each other. First, the normalized singular value curves associated with those four segments are presented in Fig. 33. All 4 cures drop sharply between the second and third singular values, an indication that all four segments are dominated by a major component.

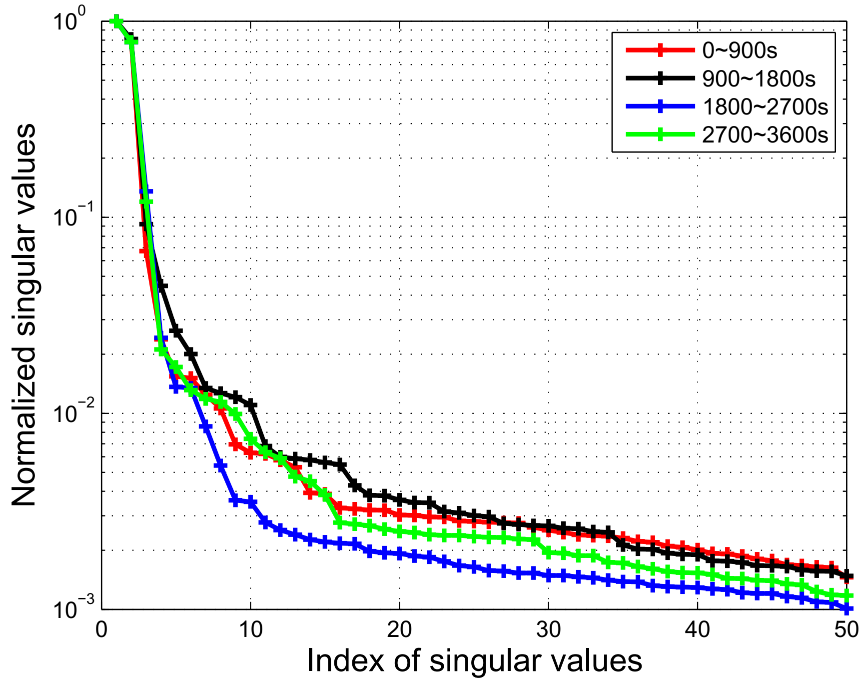

Figure 33. Normalized Singular Value curves for four segments of the Sea Test Data while using SSI method

The stabilization diagrams for those four segments are shown in Fig. 34 through Fig. 37. They all are very clean, and have a stable pole at frequency near to 0.47 Hz. For three out of those four figures, a less stable pole which is close to either 0.4 Hz or 0.3 Hz is likely associated with the dominant wave frequency.

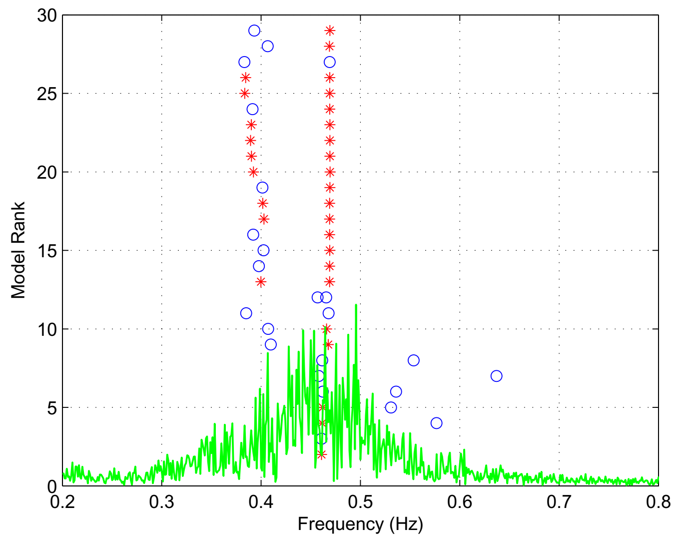

Figure 34. Stabilization diagram of segment I (from 0 to 900s) of the sea test data by using SSI

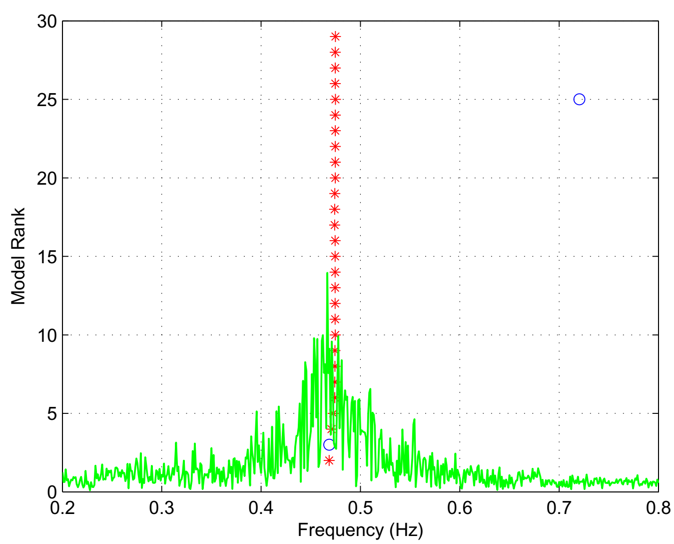

Figure 35. Stabilization diagram of segment II (from 900 to 1800s) of the sea test data by using SSI

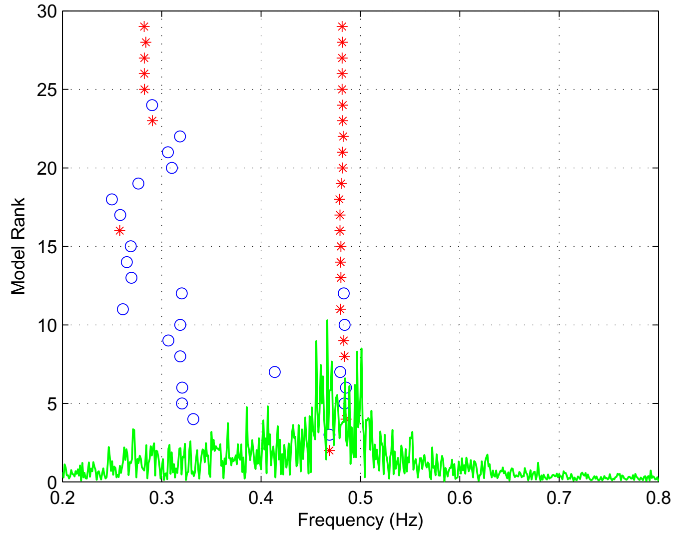

Figure 36. Stabilization diagram of segment III (from 1800 to 2700s) of the sea test data by using SSI

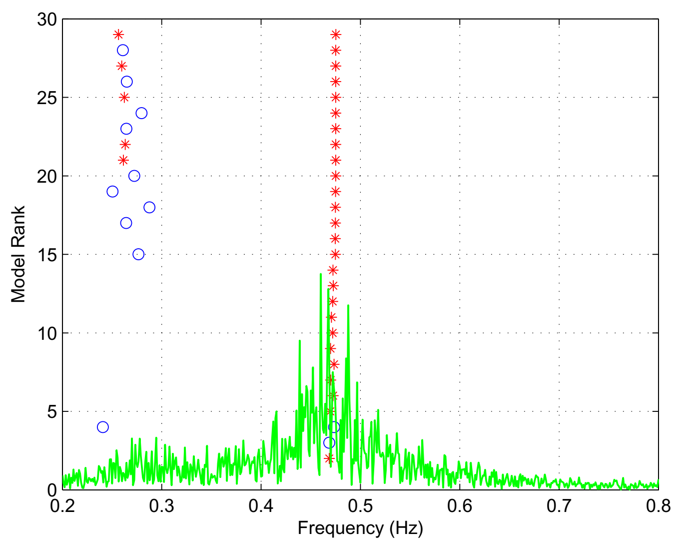

Figure 37. Stabilization diagram of segment IV (from 2700 to 3600s) of the sea test data by using SSI

Table 2 lists the estimated modal frequency and damping ratio from each of the four segments. The estimated frequencies are in excellent agreement, ranged from 0.4711 to

0.4786 Hz; the estimated damping ratios are very reasonable, ranged from 0.1450 to 0.2189. While the modal frequency would be affected by the added mass of the buoy-wave system, the damping ratio would be affected by not only the added hydrodynamic damping, but also the internal energy loss to the LEG power extraction.

Table 2. Estimated frequencies and damping ratios from four segments

Segment	I	II	III	IV
Frequency (Hz)	0.4717	0.4739	0.4786	0.4711
Damping ratio	0.2189	0.1450	0.1746	0.1804

4.4.2 Time-Frequency Domain Analysis

Because of the irregular wave motion and the highly nonlinear buoy-wave interaction, the modal parameters of the buoy-wave system are expected to be time-varying. As the modal frequency and damping ratio have been first estimated by using SSI method, Figs. 38(a) through 39(b) show the amplitude and damping ratio images for the time-frequency analysis.

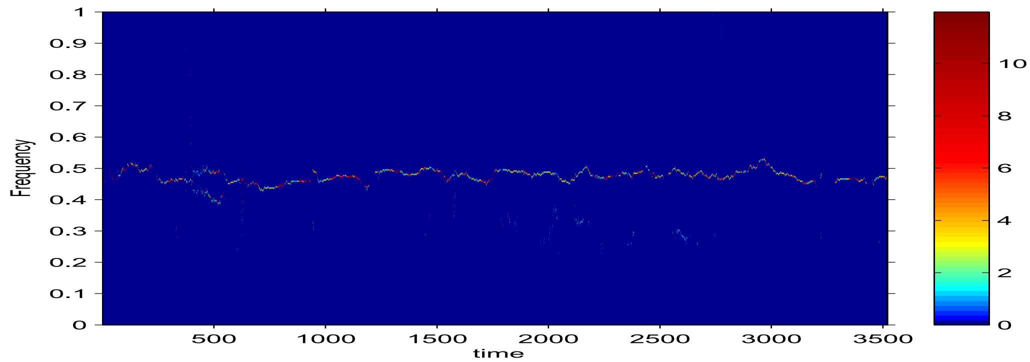

(a) Amplitude image

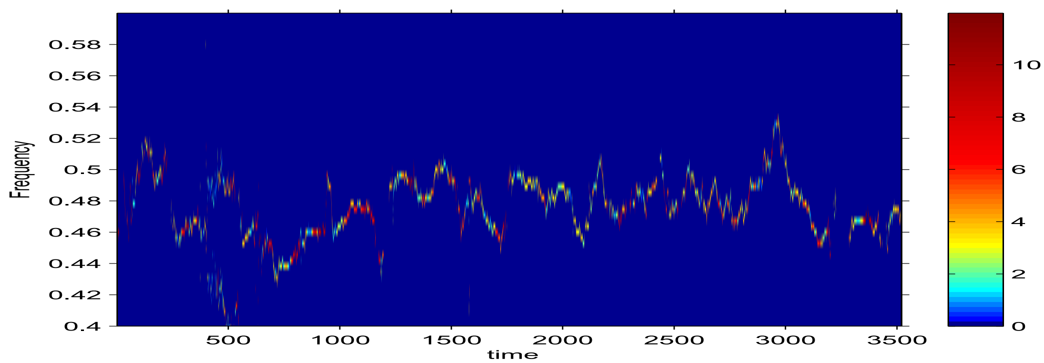

(b) Zoom in image

Figure 38. Time series of amplitude image of sea test data by SSI

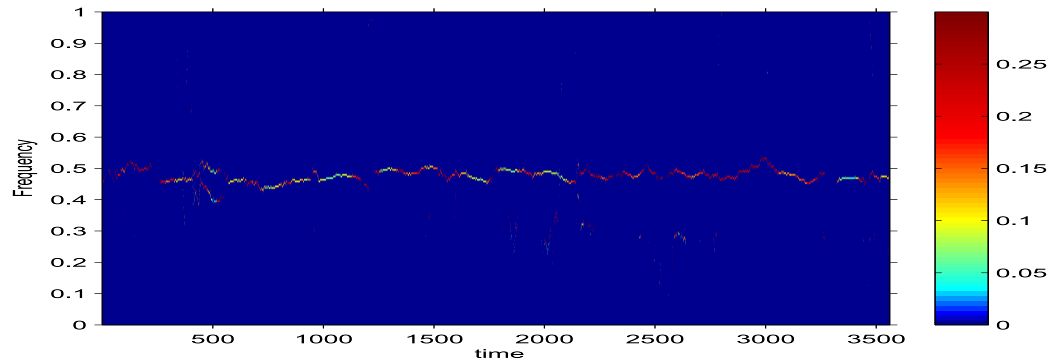

(a) Damping Image

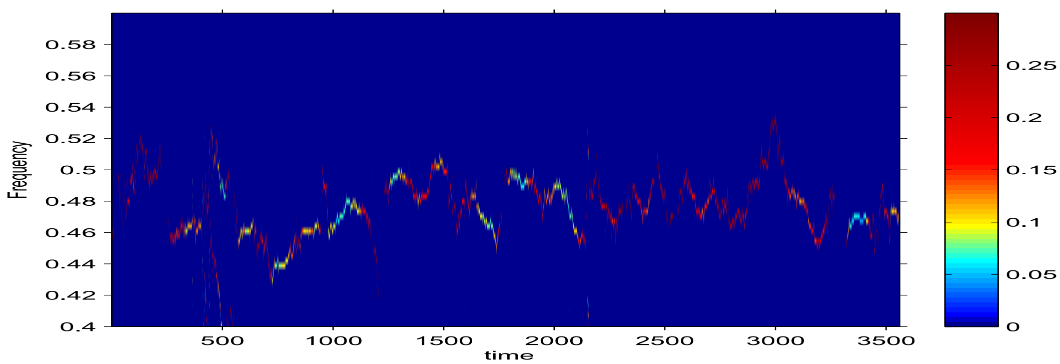

(b) Zoom in Image

Figure 39. Time series of damping image of sea test data by SSI

4.5 Summary and Discussion

In this chapter, the same star-spar buoy which had been employed for the tank testing study (in Chapter 3) was used for a sea testing study. The only different arrangement for this power-generation buoy is that its LEG was "parked" (no oscillation for the LEG device allowed) during the tank test and was in operation to generate power during the sea test. The response level of the buoy-wave system would reduce whenever there is an energy dissipation mechanism involved, and it makes no difference whether the energy dissipation is due to the hydrodynamic damping or the conversion of mechanical power to electric power through the LEG device. Due to the different arrangements for the LEG, it is reasonable that the modal damping estimated from the sea test data is larger than that estimated from the tank test data.

Using the sea test data, we conducted the signal decomposition/reconstruction, time-frequency analysis, and modal identification for the buoy-wave system in this chapter. The major findings and conclusions related to the ERA and SSI methods on signal decomposition/reconstruction, time-frequency analysis and modal identification concur with those stated in Chapter 3. First, it was demonstrated that using ERA to estimate component frequencies and damping ratios, together with a least-squares solution to compute amplitudes and phase angels, is an excellent technique for the signal decomposition/reconstruction. Second, for the time-frequency analysis, applying STFT is simple and fast, but often suffers a coarse frequency resolution and frequency leakages. In contrast, applying the ERA-based method for the time-frequency analysis can yield sharp frequencies corresponding to a small number of components. Third, SSI is a very efficient modal identification method for the sea test data. The stabilization diagram of using SSI exhibits one clean and stable pole. After breaking the whole 1-hour response signal into 4 segments, the estimated modal frequencies from these four segments are in excellent agreement with each other, ranged from 0.4711 to 0.4786 Hz. This is a little bit smaller than 0.5025 Hz estimated by using SSI for the tank test data. An explanation for the cause of the small discrepancy is that the buoy-wave system in the sea testing had a larger added (hydrodynamic) mass than the buoy-fluid system in the tank testing. The estimated damping ratios from the 4 segments are ranged from 0.1450 to 0.2189, which are significantly larger than the estimated damping ratio 0.0581 from using SSI for the tank test data. This larger damping ratio is likely caused by not only the added hydrodynamic damping, but also the internal energy loss to the LEG power extraction.

CHAPTER 5

Concluding Remarks

Understanding the dynamic characteristics of an ocean buoy through experiments is important for achieving the intended goals of its designs. The simplest technique to gain the knowledge of the dynamic characteristics of an ocean buoy is by observing the Fourier spectrum (or power spectrum) of the buoy's response. This thesis employed the eigensystem realization algorithm (ERA) and stochastic system identification (SSI) methods for estimating the modal properties of a small star-spar buoy system intended for wave energy harvesting, while response data of the buoy collected from both tank testing and sea testing were analyzed.

Traditionally, the discrete Fourier transform of a digital signal has been employed as a signal decomposition technique, as well as a modal identification technique by picking the peaks from its Fourier spectrum. However, the purposes and concepts of signal decomposition and modal identification are very different. While the performance of a signal decomposition technique would be judged based on the fitting between the reconstructed signal and the original signal, that of a modal identification technique could be judged based on whether identified modal parameters are close to the true modal parameters. When true modal parameters are unknown, the performance of a modal identification technique usually would be judged based on its stabilization diagram.

When a response signal, from either the tank test or the sea test, is modeled as the sum of many damped harmonic components, the numerical studies in this thesis demonstrated that using ERA to estimate component frequencies and damping ratios, together with a least-squares solution for getting amplitudes and phase angels, is an excellent signal decomposition technique.

Overall, SSI was found to be a very efficient modal identification method for both the tank and the sea test data. The stabilization diagram of using SSI exhibits one clean and stable pole. Although ERA has long been perceived to be an effective modal identification technique for dealing with free oscillation signal, it was found that ERA is not the best modal identification technique if the free oscillation signal has been contaminated. In dealing with the distorted free oscillation signal measured from a small tank, where the measured free oscillation signal would be affected by reflected waves, it was found that SSI outperforms ERA for modal identification.

In their theoretical derivations, both ERA and SSI methods have been under the assumption that the dynamic system is a time-invariant linear system. However, the real buoy-fluid system under investigation must be a nonlinear system, thus to apply ERA or SSI, a first approximation is to treat the dynamic system to be piecewise linear, i.e. linear within a short period. In this study, introducing a sliding window is for assuming that the system is linear within the window duration. With this sliding window, an ERA-based time-frequency analysis, in parallel to the short time Fourier transform (STFT), has been conducted. It was concluded that using ERA-based analysis could overcome the frequency resolution and leakage problems.

For the sea test data, the one-hour response signal was divided into 4 segments. From these four segments, the estimated modal frequencies by using SSI were found in excellent agreement, ranged from 0.4711 to 0.4786 Hz. This frequency range was a little bit smaller than 0.5025 Hz estimated by using SSI for the tank test data. The small discrepancy is likely because the buoy-wave system in the sea testing had a larger added (hydrodynamic) mass than the buoy-fluid system in the tank testing. The estimated damping ratios from the 4 segments are ranged from 0.1450 to 0.2189, which are significantly larger than the estimated damping ratio 0.0581 from using SSI for the tank test data. This larger damping ratio is likely caused by not only the added hydrodynamic damping, but also the internal energy loss to the LEG power extraction, noting that the power-generation buoy's LEG was "parked" during the tank test and was in operation to generate power during the sea test.

Appendix I: QR-decomposition to get a projection matrix

general formula using numerical notations $AB^\top(BB^\top)^\dagger B$

Orthogonal projections can be easily expressed in function of the $\mathbf{RQ}$ decomposition. We first treat the general case $\mathbf{A}/\mathbf{B}$, where $\mathbf{A}$ and $\mathbf{B}$ consist of any number of rows of $\mathbf{H}$, which implies that they can be expressed as linear combinations of the matrix $\mathbf{Q}^T$

$$\mathbf{H} = \begin{bmatrix} \mathbf{B} \\ \mathbf{A} \end{bmatrix} = \begin{bmatrix} \mathbf{R}_B \\ \mathbf{R}_A \end{bmatrix} \mathbf{Q}^T = \begin{bmatrix} \mathbf{R}_{11} & \mathbf{0} \\ \mathbf{R}_{21} & \mathbf{R}_{22} \end{bmatrix} \begin{bmatrix} \mathbf{Q}_1^T \\ \mathbf{Q}_2^T \end{bmatrix} \tag{36}$$

$$\begin{aligned} \mathbf{A} &= \mathbf{R}_A\mathbf{Q}^T \\ \mathbf{B} &= \mathbf{R}_B\mathbf{Q}^T \end{aligned} \tag{37}$$

we thus get the projection $\mathbf{A}$ on $\mathbf{B}$:

$$\mathscr{P} = \mathbf{A}/\mathbf{B} = \mathbf{A}\mathbf{B}^T(\mathbf{B}\mathbf{B}^T)^\dagger\mathbf{B} \tag{38}$$

Since $\mathbf{A} = \mathbf{R}_A\mathbf{Q}^T$, $\mathbf{B} = \mathbf{R}_B\mathbf{Q}^T$ and $\mathbf{Q}^T\mathbf{Q} = \mathbf{I}$, from the Eq.38 we have

$$\begin{aligned} \mathscr{P} &= (\mathbf{R}_A\mathbf{Q}^T\mathbf{Q}\mathbf{R}_B^T)(\mathbf{R}_B\mathbf{Q}^T\mathbf{Q}\mathbf{R}_B^T)^\dagger\mathbf{R}_B\mathbf{Q}^T \\ &= \mathbf{R}_A\mathbf{R}_B^T(\mathbf{R}_B\mathbf{R}_B^T)^\dagger\mathbf{R}_B\mathbf{Q}^T \end{aligned} \tag{39}$$

Note that $\mathbf{R}_B = \begin{bmatrix} \mathbf{R}_{11} & \mathbf{0} \end{bmatrix}$, we thus have $\mathbf{R}_A\mathbf{R}_B^T = \mathbf{R}_{21}\mathbf{R}_{11}^T$, $\mathbf{R}_B\mathbf{R}_B^T = \mathbf{R}_{11}\mathbf{R}_{11}^T$ and $\mathbf{R}_B\mathbf{Q}^T = \mathbf{R}_{11}\mathbf{Q}_1^T$.

Assume(for simplicity) the $\mathbf{R}_B$ is of full row rank, Eq.39 can be simplified to be

$$\begin{aligned} \mathscr{P} &= \mathbf{R}_{21}\mathbf{R}_{11}^T(\mathbf{R}_{11}\mathbf{R}_{11}^T)^{-1}\mathbf{R}_{11}\mathbf{Q}_1^T \\ &= \mathbf{R}_{21}\mathbf{Q}_1^T \end{aligned} \tag{40}$$

This suggests that the projection $\mathscr{P}$ can be obtained from $\mathbf{RQ}$-decomposition of $\mathbf{H}$.

Appendix II: Realization in modal coordinates

The state space model is written as:

$$\begin{aligned}\mathbf{x}_{k+1} &= \mathbf{A}\mathbf{x}_k + \mathbf{B}\mathbf{u}_k \\ \mathbf{y}_k &= \mathbf{C}\mathbf{x}_k\end{aligned} \tag{41}$$

Introduce the transformation between $\mathbf{x}_k$ and $\mathbf{z}_k$ as:

$$\mathbf{x}_k = \mathbf{\Psi}\mathbf{z}_k \tag{42}$$

where $\mathbf{\Psi} = [\mathbf{\Psi}_1, \mathbf{\Psi}_2, \cdots, \mathbf{\Psi}_n] \in \mathbb{R}^{n\times n}$ contains the eigenvectors of $\mathbf{A}$. It is realized that $\mathbf{z}_k$ represents the magnitude in the modal coordinates.

Substituting Eq. (42) into Eq. (41) yields

$$\begin{aligned}\mathbf{\Psi}\mathbf{z}_{k+1} &= \mathbf{A}\mathbf{\Psi}\mathbf{z}_k + \mathbf{B}\mathbf{u}_k \\ \mathbf{y}_k &= \mathbf{C}\mathbf{\Psi}\mathbf{z}_k\end{aligned} \tag{43}$$

Premultiplying $\mathbf{\Psi}^{-1}$ at the top equation of Eq. (43) leads to:

$$\begin{aligned}\mathbf{\Psi}^{-1}\mathbf{\Psi}\mathbf{z}_{k+1} &= \mathbf{\Psi}^{-1}\mathbf{A}\mathbf{\Psi}\mathbf{z}_k + \mathbf{\Psi}^{-1}\mathbf{B}\mathbf{u}_k \\ \mathbf{y}_k &= \mathbf{C}\mathbf{\Psi}\mathbf{z}_k\end{aligned} \tag{44}$$

Rewrite Eq. (44) as:

$$\begin{aligned}\mathbf{z}_{k+1} &= \mathbf{\Lambda}\mathbf{z}_k + \mathbf{B}^*\mathbf{u}_k \\ \mathbf{y}_k &= \mathbf{C}^*\mathbf{z}_k\end{aligned} \tag{45}$$

where $\mathbf{\Lambda} = \mathbf{\Psi}^{-1}\mathbf{A}\mathbf{\Psi}$, $\mathbf{B}^* = \mathbf{\Psi}^{-1}\mathbf{B}$ and $\mathbf{C}^* = \mathbf{C}\mathbf{\Psi}$.

The realization $[\mathbf{A}, \mathbf{B}, \mathbf{C}]$ associated with state variables $\mathbf{x}$ is now transformed into the realization $[\mathbf{\Lambda}, \mathbf{\Psi}^{-1}\mathbf{B}, \mathbf{C}\mathbf{\Psi}]$ in the modal coordinates.

Appendix III: Physical and State-space models

The equations of motion for an N-degree-of-freedom linear-dynamic are a set of N second-order differential equations. Let $\mathbf{M}$, $\boldsymbol{\zeta}$, $\mathbf{K} \in \mathbb{R}^{N\times N}$ be the mass, damping and stiffness matrices, respectively. These equations can be expressed in matrix notation as:

$$\mathbf{M}\ddot{\mathbf{d}}(t) + \boldsymbol{\zeta}\dot{\mathbf{d}}(t) + \mathbf{K}\mathbf{d}(t) = \mathbf{f}(t) \tag{46}$$

where $\ddot{\mathbf{d}}(t)$, $\dot{\mathbf{d}}(t)$ and $\mathbf{d}(t) \in \mathbb{R}^N$ are vectors of generalized acceleration, velocity, and displacement, respectively, and $\mathbf{f}(t) \in \mathbb{R}^N$ is the forcing function over the period of interest at certain specific locations. Let force vector $\mathbf{f}(t) = \mathbf{B}_2\mathbf{u}(t)$ be factorised into a matrix $\mathbf{B}_2 \in \mathbb{R}^{N\times m}$ describing the inputs in space and a vector $\mathbf{u}(t) \in \mathbb{R}^m$ describing the m inputs in time.

We can rewrite a first-order system of differential equation in a number of ways. Introducing

$$\mathbf{x} = \begin{bmatrix} \mathbf{d} \\ \dot{\mathbf{d}} \end{bmatrix} \tag{47}$$

we formulate a classical state space model as:

$$\dot{\mathbf{x}}(t) = \mathbf{A}_c\mathbf{x}(t) + \mathbf{B}_c\mathbf{u}(t) \tag{48}$$

where

$$\mathbf{A}_c = \begin{bmatrix} \mathbf{0} & \mathbf{I} \\ -\mathbf{M}^{-1}\mathbf{K} & -\mathbf{M}^{-1}\boldsymbol{\zeta} \end{bmatrix} \tag{49}$$

and

$$\mathbf{B}_c = \begin{bmatrix} \mathbf{0} \\ \mathbf{M}^{-1}\mathbf{B}_2 \end{bmatrix} \tag{50}$$

When the response of dynamic system is measured by l output quantities in the output vector $\mathbf{y}_t$ using sensors such as accelerometers, strain gages, etc., a matrix output equation can be expressed as:

$$\mathbf{y}(t) = \mathbf{C}\mathbf{x}(t) + \mathbf{D}\mathbf{u}(t) \tag{51}$$

where $\mathbf{C} \in \mathbb{R}^{l \times n}$ is the output matrix and $\mathbf{D} \in \mathbb{R}^{l \times m}$ is the direct transmission matrix.

Equations 48 and 51 constitute a continuous-time deterministic state-space model. When measurements are available at discrete time instants $k\triangle t$, $k \in \mathbb{N}$ with $\triangle t$, the sample time, after sampling, the state-space model looks like

$$\mathbf{x}_{k+1} = \mathbf{A}\mathbf{x}_k + \mathbf{B}\mathbf{u}_k \tag{52}$$

$$\mathbf{y}_k = \mathbf{C}\mathbf{x}_k + \mathbf{D}\mathbf{u}_k \tag{53}$$

where $\mathbf{x}_k = \mathbf{x}(k\triangle t)$ is the discrete-time state vector, $\mathbf{A} = \exp(\mathbf{A}_c \triangle t)$ is the discrete state matrix and $\mathbf{B} = [\mathbf{A} - \mathbf{I}]\mathbf{A}_c^{-1}\mathbf{B}_c$ is the discrete input matrix. In continuous time system $\mathbf{D}$ is most often $\mathbf{0}$, which is not the case in discrete time systems due to the sampling.

There are an infinite number of state-space representations that produce the same input-output description. Let a new state vector $\mathbf{z}$ be defined such that

$$\mathbf{x} = \mathbf{T}\mathbf{z} \tag{54}$$

where $\mathbf{T}$ is any nonsingular square matrix. Substitution of Eq. (54) into Eqs. (52) and (53) yields

$$\mathbf{z}_{k+1} = \mathbf{T}^{-1}\mathbf{A}\mathbf{T}\mathbf{z}_k + \mathbf{T}^{-1}\mathbf{B}\mathbf{u}_k \tag{55}$$

and

$$\mathbf{y}_k = \mathbf{C}\mathbf{T}\mathbf{z}_k + \mathbf{D}\mathbf{u}_k; \quad k = 0, 1, 2, \dots \tag{56}$$

It is obvious that the effect of the input $\mathbf{u}_k$ on the output $\mathbf{y}_k$ is unchanged for the new system, i.e., Eqs. (55) and (56). Thus, the matrices $\mathbf{T}^{-1}\mathbf{A}\mathbf{T}$, $\mathbf{T}^{-1}\mathbf{B}$, $\mathbf{C}\mathbf{T}$, and $\mathbf{D}$ in Eqs. (55) and (56) describe the same input-output relationship as the matrices $\mathbf{A}$, $\mathbf{B}$, $\mathbf{C}$, and $\mathbf{D}$ in Eqs.(52) and (53). Note that the $\mathbf{D}$ matrix does not change in the coordinate transformation, Eq.(54).

The stochastic components (noise) are included and we obtain the following discrete-time combined deterministic-stochastic state-space model:

$$\mathbf{x}_{k+1} = \mathbf{A}\mathbf{x}_k + \mathbf{B}\mathbf{u}_k + \mathbf{w}_k \tag{57}$$

$$\mathbf{y}_k = \mathbf{C}\mathbf{x}_k + \mathbf{D}\mathbf{u}_k + \mathbf{v}_k \tag{58}$$

where $\mathbf{w}_k \in \mathbb{R}^{n\times 1}$ is the process noise due to disturbances and modelling inaccuracies and $\mathbf{v}_k \in \mathbb{R}^{l\times 1}$ is the measurement noise due to sensor inaccuracy. They are both unmeasurable vector signals but we assume that they are zero mean, white and with covariance matrices:

$$\mathrm{E}\left[\begin{pmatrix} \mathbf{w}_p \\ \mathbf{v}_p \end{pmatrix} \begin{pmatrix} \mathbf{w}_q^T & \mathbf{v}_q^T \end{pmatrix}\right] = \begin{pmatrix} \mathbf{Q} & \mathbf{S} \\ \mathbf{S}^T & \mathbf{R} \end{pmatrix} \delta_{pq} \tag{59}$$

where E is the expected value operator and δ_{pq} is the Kronecker delta. The matrices $\mathbf{Q} \in \mathbb{R}^{n\times n}$, $\mathbf{S} \in \mathbb{R}^{n\times l}$ and $\mathbf{R} \in \mathbb{R}^{l\times l}$ are the covariance matrices of the noise sequences $\mathbf{w}_k$ and $\mathbf{v}_k$.

Since there are an infinite number of state-space representations, the state vector $\mathbf{x}_k \in \mathbb{R}^n$ containing the numerical values of n states does not necessarily have a direct physical interpretation. Of course, one could always find a similarity transformation of the state space model to convert the states to the modal coordinates.

The state space model associated with ERA is assuming no noise terms $\mathbf{w}_k$, $\mathbf{v}_k$, and having impulsive loading for $\mathbf{u}_k$. In the case of ambient vibration testing the input $\mathbf{u}_k$ remains unmeasured and it disappears from equation (6). The input is now implicity modelled by the noise terms $\mathbf{w}_k$, $\mathbf{v}_k$. However, the white noise assumptions of these terms cannot be omitted: it is necessary for the proofs of the system identification methods of next sections. The consequence is that if this white noise assumption is violated, for instance if the input contains some dominant frequency components in addition to white noise, these frequency components cannot be separated from the eigenfrequencies of the system and they will appear as poles of the state matrix $\mathbf{A}$.

MATLAB Files
Short Time Fourier Transform

```
%This program is the main program of plotting the STFT
    image using tank test data.
close all
clc
clear all
%--load the tank test data and remove the mean value
    --------
load tank495-4.txt
sigZZ=(tank495_4(:,4)-mean(tank495_4(:,4)))/668;
%---plot the tank test data------------------
dt=1/640
tt=1*640*dt:dt:60*640*dt;
sigZZ=sigZZ(1*640:60*640);
figure
plot(tt,sigZZ)
grid on
legend('AccelerationZ')
fc=640;
%duration of the signal
T=60;
%zero padding factor
my_zero=1;
x=sigZZ;
[spectrogram, axisf, axist]=stft(x,3200,64,fc,'blackman',
    my_zero);
```

```
figure ,imagesc(axist -5,axisf ,spectrogram)
ylabel('frequency [Hz]'),
xlabel('time [s]'),
% set(gca,'tickdir','out');
% h=get(g,'Parent');
set(gca,'YDir','normal')
colorbar;
```

```
function [spectrogram, axisf, axist] = stft(s,win_size, my_step,fc,win,zeropad)
% This MATLAB function resides in:
% http://commons.wikimedia.org/wiki/User:Alejo2083/Stft_script
% Produces the following images:
% http://commons.wikimedia.org/wiki/File:STFT_colored_spectrogram_25ms.png
% http://commons.wikimedia.org/wiki/File:STFT_colored_spectrogram_125ms.png
% http://commons.wikimedia.org/wiki/File:STFT_colored_spectrogram_375ms.png
% http://commons.wikimedia.org/wiki/File:STFT_colored_spectrogram_1000ms.pn
%
%[spectrogram, axisf, axist] = stft(s,win_size,my_step,fc,win,zeropad)
%
% calculate the spectrogram of the signal s
```

```
%
% Input s=signal to process;
% win_size= size of the window to calculate the FFT;
% my_step=shift of the window;
% fc=sampling frequency;
% win=type of window ( boxcar , hamming , blackman
    );
% zeropad=zeropadding factor;
%
%Output: spectrogram = time-frequency matrix
% axisf= vector of frequencies;
% axist= vector of time;

if nargin<6
    zeropad=1;
end
if nargin<5
    win='boxcar';
end

N=length(s);

%number of iterations
i_tot=floor((N-win_size)/my_step);

%initialization of the output matrix
```

```
spectrogram=zeros(floor(win_size*zeropad/2),i_tot);

%create the right window
if isequal(win,'boxcar')
    my_window=ones(win_size,1);
elseif isequal(win,'hamming')
    my_window=hamming(win_size);
elseif isequal(win,'blackman')
    my_window=blackman(win_size);
end
%  my_window=hamming(win_size);
my_window=my_window;

for ii=1:i_tot
    %starting index
    a=1+(ii-1)*my_step;
    %ending index
    b=win_size+(ii-1)*my_step;
    %part of the signal to be processed
    temp=s(a:b);
    %scale with the chosen window
    temp=temp.*my_window;
    %initialize the zero-padded version
    zeropadded=zeros(1,win_size*zeropad);
    %create the zero-padded vector
    zeropadded(1:win_size)=temp;
```

```
    %FFT
    zeropadded=abs(fft(zeropadded))*2/length(zeropadded);
    %get frequencies only once
    zeropadded=zeropadded(1:floor(win_size*zeropad/2));
    %store in the final matrix
    spectrogram(:,ii)=zeropadded';
end

%create axis to be used to plot the output
axisf=linspace(0,fc/2,floor(win_size*zeropad/2));
axist=linspace(win_size/fc,N/fc,ii);
```

Eigensystem Realization Algorithm

```
function [freq_Hz ,damping ,Amp,theta_complex ]= ERA_willow_damped(alpha ,dt ,sig ,LENG,Ni ,No,r_H0)
%--------------------------------------------------------------------------%
%This program is the main program to calculate the value of eigenfrequency ,
%damping , amplitude , phase angle using the ERA method.
%
% input:
%
%    sig: signals (Nt x Ns)  Nt:number of time steps; Ns= number of signals
%    dt: time interal
%    Ns=  No*Ni
%    r_H0: model order
%    No: number of output
%    Ni: number of input
%    The first No column of sig should be associated with one exitation
%    alpha: number of block rows
%    beta: number of block colums
%
% output:
%
%    freq_Hz: estimated frequency in Hz
%    damping: estimated damping factor
```

```
%     Amp: estimated amplitude (at initial time)
%     theta: estimated phase angle (radian)
%     Ref: Juang's book chapter 5; SSI paper: "reference-based stochastic
%     subspace identification for output-only modal analysis" ().
%
% ----------------------------------------------------------------------%

alpha=length(sig)/2; beta=alpha; No=1; Ni=1;

bh=block_hankel(sig,alpha,beta+1,No,Ni);% generate the block hankel matrix
H_0=bh(:,1:end-Ni);                 % eliminate the last block column
H_1=bh(:,Ni+1:end);                 % eliminate the first block column

[rowp,colp]=find(isnan(H_0));
% Find the row and column index of the rows and columns which have NaN in H(0)
[rowq,colq]=find(isnan(H_1));
% Find the row and column index of the rows and columns which have NaN in H(1)
```

```
row=[rowp;rowq];
col=[colp;colq];

rowsig=find(isnan(sig));
% Find the row index of the rows which have NaN in sig

H_0=OnDeleteMatrix(H_0,[],col);
H_1=OnDeleteMatrix(H_1,[],col);
sig=OnDeleteMatrix(sig,rowsig,[]);
% Calculate the new H(0), H(1) and sig after deleting the rows and columns which contain NaN

[u0,s0,v0]=svd(H_0);   % SVD of H(0)
sigma0=diag(s0);       % singular values of the original Hankel matrix
ss1=size(sigma0,1);    %ss1 is the number of singular values

%%------ the normalized singular values ----------------%%
for i=1:ss1
    normalize1(i)=sigma0(i)/max(sigma0);
end
size(normalize1);

%%----rank estimation of the original Hankel matrix----%%
figure
```

```
semilogy(1:ss1,normalize1(1:ss1),'r-+','linewidth',2)
hold on
grid on
xlabel('Index of singular values','FontSize',14)
ylabel('Normalized singular values','FontSize',14)
grid on
xlim([0 50])

%---------- model order determination --------------------%%
r_H0=input('model order=  ')% this is the model order you set.
[u1,s1,v1]=svds(H_0,r_H0);    %ERA

%%----------calculate A, B and C------------------------------%%
A=inv(s1).^(1/2)*u1'*H_1*v1*inv(s1).^(1/2);
B=s1.^(1/2)*v1';
B=B(:,[1:Ni]);
C=u1*s1.^(1/2);
C=C([1:No],:);

%%----------calculate lamda --------------%%
[VV,lamda] = eig(A);
lamda_c=diag(lamda);
lamda_c=log(lamda_c)/dt;
%[lamda_c,index2]=sort(lamda_c);
lambda=lamda_c;
```

```

%-------------calculate gamma-----------------%
for m=1:length(sig)
    YY(m,:)=exp((m-1)*dt.*lamda_c);% YY is the coefficient matrix
end
if length(sig)<r_H0
    error('More data points are needed!')
end
if length(sig)==r_H0
    gamma=inv(YY)*sig;
else if length(sig)>r_H0
        gamma=inv(YY'*YY)*YY'*sig;
    end
end

%---------pick just one form every conjugate pair of lambda ------%
index1_complex=1;index1_real=1;lambda_complex=[];lambda_real=[];
if  abs(abs(lambda(1))-abs(lambda(2)))<1e-10
    lambda_complex(1)=lambda(1);
    index1_complex=index1_complex+1;
elseif  abs(abs(lambda(1))-abs(lambda(2)))>1e-10
        lambda_real(1)=lambda(1);
        index1_real=index1_real+1;
```

```
end
for m=2:length(lambda)-1
    if abs(abs(lambda(m))-abs(lambda(m-1)))>1e-10 & abs(
        abs(lambda(m))-abs(lambda(m+1)))<1e-10
        lambda_complex(index1_complex)=lambda(m);
        index1_complex=index1_complex+1;
    elseif abs(abs(lambda(m))-abs(lambda(m-1)))>1e-10 &
        abs(abs(lambda(m))-abs(lambda(m+1)))>1e-10
            lambda_real(index1_real)=lambda(m);
            index1_real=index1_real+1;
    end
end
if abs(abs(lambda(end))-abs(lambda(end-1)))>1e-10
    lambda_real(index1_real)=lambda(end);
end
lambda=[lambda_real lambda_complex];


%-------pick just one form every conjugate pair of gamma
    -------%
index2_complex=1;index2_real=1;gamma_complex=[];gamma_real
    =[];
if  abs(abs(gamma(1))-abs(gamma(2)))<1e-10
    gamma_complex(1)=gamma(1);
    index2_complex=index2_complex+1;
elseif  abs(abs(gamma(1))-abs(gamma(2)))>1e-10
```

```
            gamma_real(1)=gamma(1);
            index2_real=index2_real+1;
end
for m=2:length(gamma)-1
      if abs(abs(gamma(m))-abs(gamma(m-1)))>1e-10 & abs(abs(
          gamma(m))-abs(gamma(m+1)))<1e-10
            gamma_complex(index2_complex)=gamma(m);
            index2_complex=index2_complex+1;
      elseif abs(abs(gamma(m))-abs(gamma(m-1)))>1e-10 & abs(
          abs(gamma(m))-abs(gamma(m+1)))>1e-10
                  gamma_real(index2_real)=gamma(m);
                  index2_real=index2_real+1;
      end
end
if abs(abs(gamma(end))-abs(gamma(end-1)))>1e-10
      gamma_real(index2_real)=gamma(end);
end
gamma=[gamma_real gamma_complex];

%------find the information of the signal components-----%
% Amplitude
Amp_real=abs(gamma_real);
Amp_complex=abs(gamma_complex);
Amp=[Amp_real Amp_complex]
%
% eigenfrequency
```

```
freq_Hz_real=imag(lambda_real)/2/pi;
freq_Hz_complex=imag(lambda_complex)/2/pi;
freq_Hz=[freq_Hz_real freq_Hz_complex]
%
% damping
damping_real=real(lambda_real);
damping_complex=real(lambda_complex);
damping=[damping_real damping_complex]
%
% phase angle
theta_complex=atan2(imag(gamma_complex),real(gamma_complex))
```

Stochastic Subspace Identification

```
function [freq_Hz ,damping ,Amp,theta_complex ]=
    SSI_pengyu_damped(i ,dt ,sig ,n)
%———————————————————————————————————————————%
%This program is the main program to calculate the value
    of eigenfrequency ,
%damping , amplitude , phase angle using the SSI method.
%
% input:
%
%     sig: signals
%     dt: time interal
%     n: model order
%     i: number of block rows

%
% output:
%
%     freq_Hz: estimated frequency in Hz
%     damping: estimated damping factor
%     Amp: estimated amplitude (at initial time)
%     theta: estimated phase angle (radian).
%
%
    ———————————————————————————————————————————%
```

```
y=sig;
fs=1/dt;
u=[]
AUXin=[]
W=[]
sil=[];
m=0;
%%%%%%%%%%%%%%%%%%%%%%%%%%%%%%%%%%%%%%%%%%%%%%%%%%%%%%%%%%%%%%%%%%%%%%%%%%
[l,ny] = size(y);if (ny < l);y = y';[l,ny] = size(y);end
j = ny-2*i+1;
Y = blkhank(y/sqrt(j),2*i,j);    % Output block Hankel
R = triu(qr(Y'))';                          % R factor
clear Y;
Rf = R((2*m+l)*i+1:2*(m+l)*i,:);            % Future outputs
Rp = [R(1:m*i,:);R(2*m*i+1:(2*m+l)*i,:)]; % Past (inputs and) outputs
Ob = [Rf(:,1:l*i),zeros(l*i,l*i)];

    [U,S,V] = svd(Ob);
    ss = diag(S);

sigma_0=diag(S);  % singular values of the original Hankel matrix

clear S;
ss1=size(sigma_0,1);
```

```
 save 'svdforstability.txt' ss1 -ascii
for w=1:ss1
    normalize1(w)=sigma_0(w)/max(sigma_0);
end
size(normalize1);

 figure
semilogy(1:ss1,normalize1(1:ss1),'r-+','linewidth',2)
hold on
grid on
xlabel('Index of singular values','FontSize',14)
ylabel('Normalized singular values','FontSize',14)
grid on
xlim([0 50])

%%%%%%%%%%%%%%%%%%%%%%%%%%%%%%%%%%%%%%%%%%%%%%%%%%%%%%%%%%%%%%%%%%%%%%%%%%%%%%%%
 n=input('System order ? ');
    U1=U(:,1:n)% Determine U1%%%%%%%%%%%%%%%%%%%% the first n

% Determine gam and gamm
gam  = U1*diag(sqrt(ss(1:n)));
gamm = gam(1:l*(i-1),:);
% The pseudo inverses
gam_inv  = pinv(gam);                    % Pseudo inverse
gamm_inv = pinv(gamm);                   % Pseudo inverse
% ***********************************
```

```

% Determine the matrices A and C
mydisp(sil,['          Computing ... System matrices A,C (Order ',num2str(n),')']);
Rhs = [  gam_inv*R((2*m+l)*i+1:2*(m+l)*i,1:(2*m+l)*i),zeros(n,l) ; ...
      R(m*i+1:2*m*i,1:(2*m+l)*i+l)];
Lhs = [          gamm_inv*R((2*m+l)*i+l+1:2*(m+l)*i,1:(2*m+l)*i+l) ; ...
      R((2*m+l)*i+1:(2*m+l)*i+l,1:(2*m+l)*i+l)];

% Solve least square
sol = Lhs/Rhs;
% Extract the system matrices A and C
A = sol(1:n,1:n);
C = sol(n+1:n+l,1:n);
res = Lhs - sol*Rhs;

 save 'res.txt' res -ascii
clear Rhs
clear Lhs
clear gamm_inv
clear gam_inv
clear gam
clear gamm
%
```

```
%%%%%%%%%%%%%%%%%%%%%%%%%%%%%%%%%%%%%%%%%%%%%%%%%%%%%%%%%%%%%%%%%%%%%%%%%%%%%%%%%%%%%%%%%%%%%%%%
r_H0 = input('System order ? ');%input('        System order
    ? ');
% r_H0 =10;
[VV, lamda] = eig(A);
lamda_c=diag(lamda);
lamda_c=log(lamda_c)/dt;
%[lamda_c,index2]=sort(lamda_c);
lambda=lamda_c;

%--------calculate gamma----------%
for m=1:length(sig)
    YY(m,:)=exp((m-1)*dt.*lamda_c);% YY is the coefficient
        matrix
end
if length(sig)<r_H0
    error('More data points are needed!')
end
if length(sig)==r_H0
    gamma=inv(YY)*sig;
else if length(sig)>r_H0
        gamma=inv(YY'*YY)*YY'*sig;
    end
end

```

```
%----------pick just one form every conjugate pair of lambda---------%
index1_complex=1;index1_real=1;lambda_complex=[];lambda_real=[];
if  abs(abs(lambda(1))-abs(lambda(2)))<1e-10
    lambda_complex(1)=lambda(1);
    index1_complex=index1_complex+1;
elseif  abs(abs(lambda(1))-abs(lambda(2)))>1e-10
        lambda_real(1)=lambda(1);
        index1_real=index1_real+1;
end
for m=2:length(lambda)-1
    if abs(abs(lambda(m))-abs(lambda(m-1)))>1e-10 & abs(abs(lambda(m))-abs(lambda(m+1)))<1e-10
        lambda_complex(index1_complex)=lambda(m);
        index1_complex=index1_complex+1;
    elseif abs(abs(lambda(m))-abs(lambda(m-1)))>1e-10 & abs(abs(lambda(m))-abs(lambda(m+1)))>1e-10
            lambda_real(index1_real)=lambda(m);
            index1_real=index1_real+1;
    end
end
if abs(abs(lambda(end))-abs(lambda(end-1)))>1e-10
    lambda_real(index1_real)=lambda(end);
end
lambda=[lambda_real lambda_complex];
```

```
%----------pick just one form every conjugate pair of gamma----------------%
index2_complex=1;index2_real=1;gamma_complex=[];gamma_real=[];
if  abs(abs(gamma(1))-abs(gamma(2)))<1e-10
    gamma_complex(1)=gamma(1);
    index2_complex=index2_complex+1;
elseif  abs(abs(gamma(1))-abs(gamma(2)))>1e-10
        gamma_real(1)=gamma(1);
        index2_real=index2_real+1;
end
for m=2:length(gamma)-1
    if abs(abs(gamma(m))-abs(gamma(m-1)))>1e-10 & abs(abs(gamma(m))-abs(gamma(m+1)))<1e-10
        gamma_complex(index2_complex)=gamma(m);
        index2_complex=index2_complex+1;
    elseif abs(abs(gamma(m))-abs(gamma(m-1)))>1e-10 & abs(abs(gamma(m))-abs(gamma(m+1)))>1e-10
            gamma_real(index2_real)=gamma(m);
            index2_real=index2_real+1;
    end
end
if abs(abs(gamma(end))-abs(gamma(end-1)))>1e-10
    gamma_real(index2_real)=gamma(end);
end
```

```
gamma=[gamma_real gamma_complex];

%----find the information of the signal components---%
% Amplitude
 Amp_real=abs(gamma_real);
 Amp_complex=abs(gamma_complex);
Amp=[Amp_real Amp_complex]
%
% eigenfrequency
 freq_Hz_real=imag(lambda_real)/2/pi;
 freq_Hz_complex=imag(lambda_complex)/2/pi;
 freq_Hz=[freq_Hz_real freq_Hz_complex]
%
% damping
 damping_real=real(lambda_real);
 damping_complex=real(lambda_complex);
 damping=[damping_real damping_complex]
%
% phase angle
 theta_complex=atan2(imag(gamma_complex),real(gamma_complex
    ))
```

Stability Diagram Plot

```
% This file is for plotting the stability diagram
%--------------INPUT--------------
% sig: the signal to be analyzed
% LENG: length of the signal sig
% L_begin: starting model order
%   dt:time interval
% alpha: the number of rows of the Hankel matrices
global Ni No
%Using the ERA method
[freq_Hz,damping,Amp,theta_complex]=ERA_willow_damped(alpha,sig,dt,LENG,Ni,No,L_begin)

pre_freq=freq_Hz;
pre_damp=damping;

for L=L_begin+1:L_end
    [freq_Hz,damping]=ERA_willow_damped(alpha,sig,LENG,Ni,No,L);
    mm=length(pre_freq);
    for j1=1:mm
        criteria1=abs(pre_freq(j1)-freq_Hz)./pre_freq(j1)<1e-2; % frequency limit
        criteria2=abs(pre_damp(j1)-damping)./pre_damp(j1)<5e-2; % damping limit
        if sum(criteria1)~=0 & sum(criteria2)~=0
```

```
            plot(pre_freq(j1),L-1,'r*') % stable
        else
            plot(pre_freq(j1),L-1,'bo')   % not stable
        end
        hold on
    end
    pre_freq=freq_Hz;
    pre_damp=damping;
end
%
xlabel('Frequency (Hz)')
ylabel('Model Rank')
grid on

%-----------plot of fourier spectrum---------------
fs=1/dt;
Af0_2=fft(sig); % fft of the signal
n2=length(Af0_2);
Af0_2=Af0_2/(n2/2);
fre_2 =[0:n2-1]*fs/n2;
Af0_2(1)=[];
Phase0_2=angle(Af0_2)*180/pi;
semilogy(fre_2(1:round(n2/2)),100*abs(Af0_2(1:round(n2/2))
    ),'b','linewidth',2)
```

Nonlinear Analysis

```
%This file is calculate the value of signals' information
    as time series
%, by 6s sliding window size and a moving distanse 20/640
    s(model order=20).
clc
clear all;
close all;
load tank495-4.txt
sigZZ=(tank495_4(:,4)-mean(tank495_4(:,4)))/668;
dt=1/640;
%---------------plot of the tank test data------------------
tt=1*640*dt:dt:60*640*dt;
sigZZ=sigZZ(1*640:60*640);
sigZZ=sigZZ-mean(sigZZ);
figure
plot(tt,sigZZ,'b')
grid on
hold on
%
r=1;
r_H0=20 %model order is equal to 20
Amp=[];
theta_complex=[];
damping=[];
freq_Hz=[];
```

```
   tic
  for  l=1:20:33901;
        sig=sigZZ(l:l+3840);
        t=tt(l:l+3840);
LENG=length(sig);
alpha=length(sig)/2;
No=1;  Ni=1;
[freq_Hz,damping,Amp,theta_complex]=ERA_willow_damped(alpha,dt,sig,LENG,Ni,No,r_H0)

%amplitude
Amp(r,:)=2*Amp
%frequency
freq_Hz(r,:)=freq_Hz
%damping
damping(r,:)=-damping;
%phase  angle
theta_complex(r,:)=atan2(imag(gamma_complex),real(gamma_complex))

r=r+1
  end
  toc
```

Image plot of ERA and SSI

```
% This file is the amplitude image plot by ERA and SSI method when model order is equal to 10.
clc
close all
AMP=Amp_complex;
FREQ=freq_Hz;
[no_t_step,no_comp] = size(AMP);

%--------------------------------remove unreasonable components--------------------------------------------
% [nr,nc]=size(AMP)
% for j=1:nr
%     for i=1:nc
%         ii=AMP(j,i);
%       if ii >0.35;
%       FREQ(j,i)=0;
%       AMP(j,i)=0;
%       elseif ii <-0.05;
%       FREQ(j,i)=0;
%       AMP(j,i)=0;
%       end
%     end
% end
% % % % % % % % % %
% [nr,nc]=size(FREQ)
```

```
% for j=1:nr
%     for i=1:nc
%         ii=FREQ(j,i);
%        if ii >10;
%        FREQ(j,i)=0;
%        AMP(j,i)=0;
%        elseif ii <0.47;
%        FREQ(j,i)=0;
%        AMP(j,i)=0;
%         end
%     end
% end
%
    ----------------------------------------------------------------------------------------------------

t_start =1;
t_end =54;
dt =(t_end - t_start) / (no_t_step -1);
no_comp=5; % how many components are there.
f_max=max(max(FREQ));
f_min=min(min(FREQ));

delta_f=f_max-f_min;
if f_min < -1e-1
   error('Error: negative In_frequency appears!');
```

```
end
freq_bands=8000;
h1=zeros(no_t_step-1, freq_bands+1);
p=round(freq_bands*(FREQ-f_min)/delta_f)+1; % p will be between 1 and (freq_bands+1)
for j1=1:no_t_step-1
    for i1=1:no_comp
        ii1=p(j1,i1);
        h1(j1,ii1)=h1(j1,ii1)+AMP(j1,i1);
    end
end
[nx,ny]=size(h1);

Hz=linspace(f_min,f_max,ny)';
time=linspace(t_start,t_end,nx)';
h1=flipud(rot90(h1));
figure
g=imagesc(time,Hz,h1);
colorbar
xlabel('Time (s)')
ylabel('Frequency')
set(gca,'tickdir','out');
h=get(g,'Parent');
set(h,'Ydir','normal');
xlabel(' time')
```

LIST OF REFERENCES

[1] S. T. Grilli, A. R. Grilli, S. P. Bastien, R. B. S. Jr, and M. L. Spaulding, "Small buoys for energy harvesting: Experimental and numerical modeling studies." in *Proceedings of the Twenty-first International Offshore and Polar Engineering Conference*, 2011.

[2] W. J. Palm, Ed., *Mechanical Vibration, 2^{nd} ed.* John Wiley and Sons, Inc, 1986.

[3] A. Cunha and E. Caetano, "Experimental modal analysis of civil engineering structures," *Sound and Vibration*, pp. 12–20, 2006.

[4] L. Mangal, V. Idichandy, and C. Ganapathy, "Structural monitoring of offshore platforms using impulse and relaxation response," *Ocean Engineering*, vol. 28, pp. 689–705, 2011.

[5] H. Li, J. Wang, and S. L. J. Hu, "Using incomplete modal data for damage detection in offshore jacket platform structures," *Ocean Engineering*, vol. 35, pp. 1793–1799, 2008.

[6] E. O. Brigham, Ed., *The fast fourier transform and its application*. Prentice-Hall, Engelwood Cliffs, Engelwood Cliffs, 1988.

[7] B. Peeters and G. D. Roeck, "Comparison of system identification methods using operational data of a bridge test," in *In Proceedings of The International Conference on Noise and Vibration Engineering*, 1998, pp. 923–930.

[8] M. Greitans, "Adaptive stft-like time-frequency analysis from arbitrary distributed signal samples," in *International Workshop on Sampling Theory and Application*, 213-eoa, Ed., 2005.

[9] J.-N. Juang, *Applied System Identification*, J.-N. Juang, Ed. Upper Saddle River, NJ 07458: Prentice Hall PTR, 1994.

[10] B. L. Ho and R. E. Kalman, "Effective construction of linear, state-variable models from input/output functions," *Regelungstechnik*, vol. 14 12, p. 545C548., 1966.

[11] G. Strang, Ed., *Linear Algebra and Its Application, 3^{rd} ed.* Harcourth Brace Jovanovich, Inc.,, 1988.

[12] B. Peeters and G. DeRoeck, "Reference-based stochastic subspace identification for output-only modal analysis," *Mechanical Systems and Signal Processing*, vol. 13(6), pp. 855–878, 1999.

[13] P. VanOverschee and B. DeMoor, "Subspace algorithms for the stochastic identification problem," *Automatica*, vol. 29(3), pp. 649–660, 1993.

[14] J. Xin, S. L. J. Hu, and H. Li, "Experimental modal analysis of jacket-type platforms using data-driven stochastic subspace identification method," in *Proceedings of the ASME 2012 31st International Conference on Ocean, Offshore and Arctic Engineering*, 2012.

[15] S.-L. J. Hu, X. Bao, and H. Li, "Model order determination and noise removal for modal parameter estimation," *Mechanical Systems and Signal Processing*, vol. 24, pp. 1605–1620, 2010.

[16] S. L. Marple, Ed., *Digital Spectral Analysis with Applications*. Prentice-Hall, Engelwood Cliffs, Engelwood Cliffs, NJ, 1987, 1987.

BIBLIOGRAPHY

A. Cunha and E. Caetano, "Experimental modal analysis of civil engineering structures," *Sound and Vibration*, pp. 12–20, 2006.

B. L. Ho and R. E. Kalman, "Effective construction of linear, state-variable models from input/output functions," *Regelungstechnik*, vol. 14 12, p. 545C548., 1966.

B. Peeters and G. D. Roeck, "Comparison of system identification methods using operational data of a bridge test," in *In Proceedings of The International Conference on Noise and Vibration Engineering*, 1998, pp. 923–930.

B. Peeters and G. DeRoeck, "Reference-based stochastic subspace identification for output-only modal analysis," *Mechanical Systems and Signal Processing*, vol. 13(6), pp. 855–878, 1999.

D. Tufts and A. Shah, "Estimation of a signal waveform from noisy data using low-rank approximation to a data matrix," *IEEE Trans. Signal Process.*, vol. 41, no. 4, pp. 1716–1721, 1993.

E. O. Brigham, Ed., *The fast fourier transform and its application*. Prentice-Hall, Engelwood Cliffs, Engelwood Cliffs, 1988.

G. Strang, Ed., *Linear Algebra and Its Application, 3^{rd} ed.* Harcourth Brace Jovanovich, Inc.,, 1988.

H. Li, J. Wang, and S. L. J. Hu, "Using incomplete modal data for damage detection in offshore jacket platform structures," *Ocean Engineering*, vol. 35, pp. 1793–1799, 2008.

I. Markovsky and S. V. Huffel, "Overview of total least squares methods," *Signal Processing*, vol. 87, no. 10, pp. 2283–2302, 2007.

I. S.R., "Application of random time domain analysis to dynamic flight measurements," *Shock and Vibration Bullatin*, vol. Vol.49/2,, pp. 165–170., 1979.

J. J. N and P. R. S., "An eigensystem realization algorithm for modal paremeter identification and modal reduction," *Control,and Dynamics*, pp. 620–627., 1985.

J.-N. Juang, *Applied System Identification*, J.-N. Juang, Ed. Upper Saddle River, NJ 07458: Prentice Hall PTR, 1994.

J. Xin, S. L. J. Hu, and H. Li, "Experimental modal analysis of jacket-type platforms using data-driven stochastic subspace identification method," in *Proceedings of the ASME 2012 31st International Conference on Ocean, Offshore and Arctic Engineering*, 2012.

L. Mangal, V. Idichandy, and C. Ganapathy, "Structural monitoring of offshore platforms using impulse and relaxation response," *Ocean Engineering*, vol. 28, pp. 689–705, 2011.

M. Greitans, "Adaptive stft-like time-frequency analysis from arbitrary distributed signal samples," in *International Workshop on Sampling Theory and Application*, 213-eoa, Ed., 2005.

M. MartInez, "Experimental modal analysis in offshore platforms," in *Proceedings of the International Modal Analysis Conference & Exhibit*, 213-eoa, Ed., 1991.

N. Maia, J. Silva, J. He, N. Lieven, R.-M. Lin, G. Skingle, W. To, and A. Urgueira, *Theoretical and Experimental Modal Analysis*, N. Maia and J. Silva, Eds. Taunton, Somerset, England: Research Studies Press, 1997.

N. R.Brincker, P.Andersen, "Output-only modal testing of a car body subject to engine excitation." in *Proc.of the 18th International Modal Analysis Conference,San Antonio,Texas,USA*, 2000:, p. 786 792.

P. VanOverschee and B. DeMoor, *Subspace Identification for Linear System :Theory - Implementation - Applications*. Kluwer Academic Publishers Boston/London/-Dordrecht, 1996.

P. VanOverschee and B. DeMoor, "Subspace algorithms for the stochastic identification problem," *Automatica*, vol. 29(3), pp. 649–660, 1993.

S.-L. J. Hu, X. Bao, and H. Li, "Model order determination and noise removal for modal parameter estimation," *Mechanical Systems and Signal Processing*, vol. 24, pp. 1605–1620, 2010.

S. L. Marple, Ed., *Digital Spectral Analysis with Applications*. Prentice-Hall, Engelwood Cliffs, Engelwood Cliffs, NJ, 1987, 1987.

S. T. Grilli, A. R. Grilli, S. P. Bastien, R. B. S. Jr, and M. L. Spaulding, "Small buoys for energy harvesting: Experimental and numerical modeling studies." in *Proceedings of the Twenty-first International Offshore and Polar Engineering Conference*, 2011.

The MathWorks, *Control system toolbox user's guide*, The MathWorks Inc., Natic, MA, 2004.

W. J. Palm, Ed., *Mechanical Vibration,* 2^{nd} *ed.* John Wiley and Sons, Inc, 1986.